

R. C. Batra · M. Porfiri · D. Spinello

Free and forced vibrations of a segmented bar by a meshless local Petrov–Galerkin (MLPG) formulation

Published online: 14 March 2006
© Springer-Verlag 2006

Abstract We use the meshless local Bubnov–Galerkin (MLPG6) formulation to analyze free and forced vibrations of a segmented bar. Three different techniques are employed to satisfy the continuity of the axial stress at the interface between two materials: Lagrange multipliers, jump functions, and modified moving least square basis functions with discontinuous derivatives. The essential boundary conditions are satisfied in all cases by the method of Lagrange multipliers. The related mixed semidiscrete formulations are shown to be stable, and optimal in the sense that the ellipticity and the inf-sup (Babuška-Brezzi) conditions are satisfied. Numerical results obtained for a bimaterial bar are compared with those from the analytical, and the finite element methods. The monotonic convergence of first two natural frequencies, first three mode shapes, and a static solution in the L^2 , and H^1 norms is shown. The relative error in the numerical solution for a transient problem is also very small.

Keywords MLPG method · Material discontinuities · Inf-sup condition · Convergence analysis · Segmented bar

1 Introduction

Recently, considerable research in computational mechanics has been devoted to the development of meshless methods such as the element-free Galerkin [10], hp-clouds [12], the reproducing kernel particle [20], the smoothed particle hydrodynamics [21], the diffuse element [25], the partition of unity finite element [23], the natural element [31], meshless Galerkin using radial basis functions [34], the meshless local Petrov–Galerkin (MLPG) [3], the modified smoothed particle hydrodynamics (MSPH) [35], the symmetric smoothed particle hydrodynamics (SSPH) [36], and the collocation

method using radial basis functions [15]. All of these methods, except for the MLPG, the collocation, the SSPH, and the MSPH, are not truly meshless since the use of shadow elements is inevitable for evaluating integrals in the governing weak formulations. Two recent books [2, 19], have summarized these and other meshless methods. The main objective of the meshless methods is to get rid of, or at least alleviate the difficulty of meshing and remeshing the entire structure by adding or deleting nodes at desired locations instead. Meshless methods may also alleviate some other problems associated with the finite element method (FEM), such as locking and element distortion. In many applications, they provide smooth, and accurate approximate solutions with a reduced number of nodes.

For a body made of two or more materials, the derivative of displacements in the direction normal to the interface between two materials must be discontinuous in order for surface tractions there to be continuous. For the analysis of the linear elastostatic problems by the EFG method, Cordes and Moran [11] used the method of Lagrange multipliers, Krongauz and Belytschko [17] employed a special jump function at the line or the surface of discontinuity, and Noguchi and Sachiko [26] modified the moving least square (MLS) basis functions so that their derivative jumps at desired locations. Whereas a two-dimensional (2-D) static problem was analyzed by Krongauz and Belytschko [17], a 1-D static problem was scrutinized by Cordes and Moran [11].

The MLPG method is based on a local weak formulation of governing equations, and employs meshless interpolations for both the trial and the test functions, while a background mesh is employed in the EFG method. Furthermore, in the MLPG formulation, the domains of integration may either overlap or their union may not equal the domain occupied by the body, and the trial functions are constructed by using techniques (e.g., the MLS [18] approximation, the radial basis functions [15]) which rely on locations of scattered points in the body. In the Petrov–Galerkin formulation, test functions may be chosen from a space different from the space of trial functions; in this way, depending upon the choice of the test function, and the employment of a local symmetric or local

R. C. Batra (✉) · M. Porfiri · D. Spinello
Department of Engineering Science and Mechanics MC 0219,
Virginia Polytechnic Institute and State University,
Blacksburg, VA 24061, USA
E-mail: rbatra@vt.edu, mporfiri@vt.edu, dspinell@vt.edu

asymmetric weak form, Atluri and Shen [2] proposed six variants, namely MLPG1, MLPG2, ..., MLPG6, of the MLPG method. In MLPG6, the local symmetric Bubnov–Galerkin formulation, the test function for each subdomain is chosen to be the MLS basis function associated to the related node.

Gu and Liu [13] used the MLPG method in the analysis of free and forced vibrations of solids; the method has been extended by Qian et al. [27, 28, 30] to study free, and forced vibrations of a thick rectangular plate modeled by the higher-order shear and normal deformable plate theory [6, 32]. Batra et al. [8] have compared the performance of two MLPG formulations in the analysis of a parabolic 1-D problem, i.e., the axisymmetric transient heat conduction in a bimetallic disk with the material discontinuity treated either by the method of Lagrange multipliers or the jump function [9, 17]. Note that no waves propagate in a parabolic problem. However, waves propagate in a hyperbolic problem, and may be reflected and refracted at the interface between the two materials.

In this paper, we use the MLPG6 formulation, and compare the performance of the three aforementioned techniques to account for material discontinuities in the analysis of free, and forced vibrations of a segmented bar. As a sample problem we consider a clamped-free bimaterial bar, although the approach is also suitable for other boundary conditions, and segmented bars made of more than two materials. The essential (i.e., displacement) boundary condition is imposed in all cases by introducing a Lagrange multiplier; this technique was used by Warlock et al. [33] and Batra and Wright [7] to satisfy contact conditions at a rough surface. Following the idea developed by Andreus et al. [1] for a beam, it is shown that the MLPG6 numerical solution is stable and optimal by showing that the related mixed formulations satisfy the ellipticity and the inf-sup conditions (see [5]). Numerical results are compared with analytical and FE solutions. In particular, the convergence with an increase in the number of nodes of the first two eigenfrequencies, first three mode shapes, and a static solution are shown, revealing a monotonically decreasing trend at a rate faster than that obtained with the FE method. The transient response to an axial traction of finite duration applied at one end of the bar is shown to match very well with the analytical solution of the problem.

The rest of the paper is organized as follows. In Sect. 2 we review the basic formulation of the MLS basis functions, and introduce the MLS basis functions with discontinuous derivatives [26]. Section 3 gives differential equations, and initial and boundary conditions for wave propagation in a segmented elastic bar with one end clamped and the other free, and the MLPG6 formulations for the method of Lagrange multipliers, the method of jump function, and the method of MLS basis functions with discontinuous derivatives. We also very briefly discuss the numerical evaluation of domain integrals, and the method used to numerically integrate, with respect to time, the semidiscrete system of ordinary differential equations. Numerical results computed with the three methods of treating material discontinuities are discussed in Sect. 4 where the convergence of the MLPG6 solution for static deformations, and mode shapes is compared with that

of the FE solution, and the transient response to a time dependent axial traction is compared with the analytical solution of the corresponding problem. Section 5 summarizes conclusions. Analytical solutions of the problem for free, and forced vibrations of the segmented bar are given in Appendices A and B, respectively.

2 Moving least square basis functions

2.1 Moving least square approximation

The MLS approximation, proposed by Lancaster and Salkauskas [18], allows for an accurate reconstruction of a given trial function on the entire domain, from the knowledge of its values at some, suitably chosen, scattered points. Consider the differentiable scalar function w defined on domain $\Omega := [0, L]$. The generic point in Ω is denoted by x . The (fictitious) nodal values at the scattered points $\mathcal{N} = \{x_1, x_2, \dots, x_N\}$ in $\bar{\Omega}$ are collected into the N -vector $\hat{\mathbf{w}} = [\hat{w}_1 \cdots \hat{w}_N]^T$, where the superscript T indicates transposition. The global approximation w^h of w is defined as

$$w(x) \simeq w^h(x) = \mathbf{p}^T(x) \mathbf{a}(x), \quad x \in \Omega, \quad (1)$$

where

$$\mathbf{p}^T(x) = [p_1(x) \ p_2(x) \ \cdots \ p_m(x)], \quad (2)$$

is a complete monomial basis of order m . For example:

$$\begin{aligned} \mathbf{p}^T(x) &= [1 \ x], & \text{linear basis,} & \quad m = 2; \\ \mathbf{p}^T(x) &= [1 \ x \ x^2], & \text{quadratic basis,} & \quad m = 3. \end{aligned} \quad (3)$$

The m -vector $\mathbf{a}(x) = [a_1(x) \ \cdots \ a_m(x)]^T$ is composed of indeterminate coefficients, which vary with the point x in the domain Ω . At each location \bar{x} in Ω these coefficients are determined by a local least square approximation of $w(x)$ in a small neighborhood $\Omega_{\bar{x}}$ of \bar{x} . The local approximation $w_{\bar{x}}(x)$ is defined by

$$w(x) \simeq w_{\bar{x}}(x) = \mathbf{p}^T(x) \mathbf{a}(\bar{x}), \quad x \in \Omega_{\bar{x}} \subset \Omega. \quad (4)$$

Therefore, in a small neighborhood of a generic point \bar{x} the coefficients a_i are treated as the unknown constants of the classical polynomial least square approximation, and are determined by minimizing the functional $J_{\bar{x}}$ representing the weighted discrete L^2 error norm, and defined by

$$J_{\bar{x}}(\mathbf{a}) = \sum_{i=1}^N W_i(\bar{x}) [w_{\bar{x}}(x_i) - \hat{w}_i]^2. \quad (5)$$

W_i is the weight function of node i , and is a continuous positive function with compact support. In the following, weight functions which equal 1 at the location of the corresponding nodes will be used. In the literature [16] MLS basis functions obtained by using weight functions which do not satisfy this condition have been considered.

At a given location \bar{x} only few terms in the summation (5) are not zero since supports of weight functions W_i are much smaller than the size of Ω . This can be used to reduce

the memory allocations when implementing the algorithm in a computer code, and strengthens the local character of the MLS approximation. We denote by n the number of nonvanishing terms at the point \bar{x} , and emphasize that n is a function of \bar{x} . Lower bounds for the diameters of support of the weight functions are established below to assure the regularity of the MLS basis functions.

The functional $J_{\bar{x}}$ can be written in matrix notation as

$$J_{\bar{x}}(\mathbf{a}) = (\mathbf{P}\mathbf{a} - \widehat{\mathbf{w}})^T \mathbf{W}(\bar{x}) (\mathbf{P}\mathbf{a} - \widehat{\mathbf{w}}), \quad (6)$$

where \mathbf{P} is a (N, m) matrix of real numbers:

$$\mathbf{P}^T = [\mathbf{p}^T(x_1) \cdots \mathbf{p}^T(x_N)] \quad (7)$$

and \mathbf{W} is a (N, N) diagonal matrix defined by

$$\mathbf{W}(\bar{x}) = \text{DIAG} [W_1(\bar{x}) \cdots W_N(\bar{x})]. \quad (8)$$

The local nature of the MLS approximation requires that only n terms of the matrix \mathbf{W} are different from zero.

The stationarity of $J_{\bar{x}}$ with respect to \mathbf{a} yields

$$\mathbf{A}(\bar{x}) \mathbf{a}(\bar{x}) = \mathbf{B}(\bar{x}) \widehat{\mathbf{w}}, \quad (9)$$

where the (m, m) and the (m, N) matrices \mathbf{A} and \mathbf{B} are defined by

$$\mathbf{A}(\bar{x}) = \mathbf{P}^T \mathbf{W}(\bar{x}) \mathbf{P}, \quad \mathbf{B}(\bar{x}) = \mathbf{P}^T \mathbf{W}(\bar{x}). \quad (10)$$

We note that matrices \mathbf{A} and \mathbf{B} depend on the spatial coordinate \bar{x} only through the weight functions, since \mathbf{P} is a matrix of real numbers. Solving Eq. (9) for \mathbf{a} , and substituting for \mathbf{a} in the global approximation (1) we get the MLS approximation

$$w^h(x) = \mathbf{P}^T(x) \mathbf{A}^{-1}(x) \mathbf{B}(x) \widehat{\mathbf{w}}, \quad (11)$$

which, upon introducing the vectors of basis functions $\boldsymbol{\psi}(x)$, can be expressed as

$$w^h(x) = \boldsymbol{\psi}(x)^T \widehat{\mathbf{w}}, \quad (12)$$

with

$$\boldsymbol{\psi} = [\psi_1 \dots \psi_N]^T. \quad (13)$$

The basis functions are computed from Eqs. (10) and (11) as

$$\boldsymbol{\psi}(x) = \mathbf{P}(x)^T \mathbf{A}^{-1}(x) \mathbf{P}^T \mathbf{W}(x). \quad (14)$$

We emphasize that for an arbitrary node x_i the fictitious nodal value does not equal the actual nodal value of the approximating function, i.e., $w^h(x_i) \neq \widehat{w}_i$.

The MLS expansion (12) is well defined only if the matrix \mathbf{A} in (10) is non-singular. It can be seen that this is the case if and only if the rank of the $n \times m$ matrix $\mathbf{P}_{\bar{x}}$, obtained from \mathbf{P} by deleting rows corresponding to those nodes whose weight function vanishes at \bar{x} , equals m . Obviously, a necessary condition for a well-defined MLS approximation is that at least m nodal weight functions do not vanish at \bar{x} . However, this condition is not sufficient (see [4]).

The smoothness of the MLS trial functions is completely determined by the smoothness of the weight functions, since the polynomial basis is infinitely differentiable. If α indicates the minimum order of differentiability of all weight functions, then from (10) it is evident that the trial functions are

at least α times differentiable. In the following, we consider weight functions that are at least once continuously differentiable everywhere in Ω .

In the analysis, the computation of the derivative of the MLS basis functions in (14) is needed. To save computational effort, it is worthwhile to compute explicitly the first derivative of the inverse of the matrix \mathbf{A} with respect to the coordinate x from the identity:

$$\mathbf{A}\mathbf{A}^{-1} = \mathbf{1}; \quad (15)$$

hence

$$(\mathbf{A}^{-1})' = -\mathbf{A}^{-1} \mathbf{A}' \mathbf{A}^{-1}, \quad (16)$$

where the prime implies derivative with respect to x . Therefore, only the knowledge of the weight functions, and their derivative is needed to compute the derivative of \mathbf{A}^{-1} .

In the literature (see e.g., [2]), fourth-order spline and Gauss weight functions are widely used; here, we employ the fourth-order spline weight function:

$$W_i(x) = \begin{cases} 1 - 6 \left(\frac{d_i}{r_i}\right)^2 + 8 \left(\frac{d_i}{r_i}\right)^3 - 3 \left(\frac{d_i}{r_i}\right)^4, & d_i \leq r_i \\ 0, & d_i > r_i \end{cases}, \quad (17)$$

where $d_i = |x - x_i|$ is the distance from node x_i to point x , and r_i is the radius of support of the weight function W_i .

2.2 Modified MLS basis functions with discontinuous derivatives

Let a material interface be located at the point $a \in (0, L)$ in the global domain $\Omega = [0, L]$, and let a node be located at $x = a$. Furthermore, we denote by N_1 and N_2 the number of nodes whose location x_j satisfies the condition $x_j \leq a$, $x_j > a$ respectively, and with n_1 and n_2 the number of nodes whose location x_j satisfies the condition $a - r_{N_1} < x_j \leq a$, $a < x_j < a + r_{N_1}$, respectively. Therefore, n_1 and n_2 equal the number of nodes in the domain of influence of the weight function W_{N_1} associated with the interface node $x_{N_1} = a$, placed respectively to the left, and to the right of the interface. In order to modify the basis functions in the domain of influence of the weight function W_{N_1} in such a way that all basis functions which are nonzero at the interface are continuous but have discontinuous derivative, we consider the following global approximation of the function w in the region $(a - r_{N_1}, a + r_{N_1})$:

$$w^h(x) = \begin{cases} \mathbf{p}_1^T(x) \mathbf{b}(x), & x \in (a - r_{N_1}, a) \\ \mathbf{p}_2^T(x) \mathbf{b}(x), & x \in (a, a + r_{N_1}) \end{cases}, \quad (18)$$

where

$$\mathbf{p}_1^T(x) = [1 \ x - a \ 0 \ (x - a)^2 \ 0 \ \cdots \ (x - a)^{m-1} \ 0], \quad (19)$$

$$\mathbf{p}_2^T(x) = [1 \ 0 \ x - a \ 0 \ (x - a)^2 \ \cdots \ 0 \ (x - a)^{m-1}],$$

and

$$\mathbf{b}(x) = [b_0(x) \ b_{1,1}(x) \ b_{2,1}(x) \ \cdots \ b_{1,m-1}(x) \ b_{2,m-1}(x)]. \quad (20)$$

For example, for $m = 2$ one gets

$$w^h(x) = \begin{cases} b_0(x) + (x-a)b_{1,1}(x), & x \leq a \\ b_0(x) + (x-a)b_{2,1}(x), & x > a \end{cases} \quad (21)$$

Therefore, the weighted discrete L^2 error norm to be minimized is [see Eq. (5)]

$$J_{\bar{x}}(\mathbf{b}) = \sum_{i=1}^{n_1} W_i(\bar{x}) [\mathbf{p}_1^T(x_i) \mathbf{b}(\bar{x}) - \hat{w}_i]^2 + \sum_{i=n_1+1}^{n_1+n_2} W_i(\bar{x}) [\mathbf{p}_2^T(x_i) \mathbf{b}(\bar{x}) - \hat{w}_i]^2, \quad (22)$$

$\bar{x} \in (a - r_{N_1}, a + r_{N_1})$, whose stationarity with respect to the argument gives Eq. (10) with

$$\mathbf{A}(\bar{x}) = \sum_{i=1}^{n_1} W_i(\bar{x}) \mathbf{p}_1(x_i) \mathbf{p}_1^T(x_i) + \sum_{i=n_1+1}^{n_1+n_2} W_i(\bar{x}) \mathbf{p}_2(x_i) \mathbf{p}_2^T(x_i), \quad (23)$$

$$\mathbf{B}(\bar{x}) = [W_1(\bar{x}) \mathbf{p}_1(x_1), \dots, W_{n_1}(\bar{x}) \mathbf{p}_1(x_{n_1}), W_{n_1+1}(\bar{x}) \mathbf{p}_2(x_{n_1+1}), \dots, W_{n_1+n_2}(\bar{x}) \mathbf{p}_2(x_{n_1+n_2})].$$

Solving for \mathbf{b} we obtain

$$\mathbf{b}(x) = \mathbf{A}^*(x) \mathbf{B}(x), \quad (24)$$

where \mathbf{A}^* is the pseudoinverse of matrix \mathbf{A} . Indeed, assuming that at every evaluation point x there are at least m nonvanishing weight functions, for the null space of the $(2m - 1 \times 2m - 1)$ matrix \mathbf{A} the following holds:

$$0 \leq \dim \ker \mathbf{A} \leq m - 1. \quad (25)$$

When $\dim \ker \mathbf{A} = 0$, \mathbf{A} is invertible, and its inverse and pseudoinverse coincide. However, when $\dim \ker \mathbf{A} > 0$, there are as many zero rows and columns in \mathbf{A} as the number of vanishing weight functions at x ; in this case the nonzero entries of the pseudoinverse are equal to the entries of the matrix obtained from \mathbf{A} by deleting its zero rows and columns. Note that the corresponding rows of the matrix \mathbf{B} are also zero; therefore Eq. (24) states that the related entries in the vector \mathbf{b} are zero.

For 11 uniformly distributed nodes in the domain $[0, L]$ with the interface between two materials located at $a = L/2$ or at node 6, the modified MLS basis functions for nodes 1 through 6 are plotted in Fig. 1a–f, where we have set $m = 2$, $r_i = 3L/10$, and two nodes in the radius of support of each weight function. We emphasize that, in this approach, the weight functions are not modified, while all basis functions in the domain of influence of the weight function W_{N_1} are modified due to the introduction of the discontinuous monomial basis (19) in the region $(a - r_{N_1}, a + r_{N_1})$, which affects matrices \mathbf{A} and \mathbf{B} in the same region, and therefore the MLS basis functions. Even though the weight functions in Eq. (22) are non-negative, the basis functions may assume negative values. Also, a basis function is non-zero at more than one node. It is clear that basis functions for nodes in the domain of influence of the weight function W_6 (i.e., for nodes 4, 5, and 6), have discontinuous derivative at node 6.

3 Formulation of the problem

3.1 Governing equations

We study wave propagation in a segmented bar of length L with the left¹ segment of length a made of one material, and the right one of length $L - a$ made of a different material (Fig. 2); E_i and ρ_i , $i = 1, 2$, are, respectively, Young's modulus, and the volumetric mass density of the material constituting the left, and the right parts. As an example problem, the right end of the bar is clamped, and a time dependent axial traction $p(t)$ is applied at the left end. By assuming a uniform cross section, governing equations are

$$\rho_1 \ddot{w}_1(x, t) - E_1 w_1''(x, t) = 0, \quad x \in (0, a), \quad t > 0, \quad (26)$$

$$\rho_2 \ddot{w}_2(x, t) - E_2 w_2''(x, t) = 0, \quad x \in (a, L), \quad t > 0, \quad (27)$$

with boundary conditions

$$E_1 w_1'(0, t) = p(t), \quad (28)$$

$$w_1(a, t) = w_2(a, t), \quad (29)$$

$$E_1 w_1'(a, t) = E_2 w_2'(a, t), \quad (30)$$

$$w_2(L, t) = 0. \quad (31)$$

We assume homogeneous initial conditions

$$w_1(x, 0) = w_2(x, 0) = 0, \quad \dot{w}_1(x, 0) = \dot{w}_2(x, 0) = 0. \quad (32)$$

Here, $w_i(x, t)$ is the longitudinal displacement of point x in the i -th segment of the bar; a superimposed dot means partial differentiation with respect to time t , while a prime means partial differentiation with respect to x . The global axial displacement field, w , is given by

$$w(x, t) = \begin{cases} w_1(x, t), & x \in (0, a) \\ w_2(x, t), & x \in (a, L) \end{cases}, \quad (33)$$

and a similar notation will be adopted for the global volumetric mass density, and Young's modulus.

Equations (29) and (30) state the continuity of the displacement, and of the axial stress at the interface. We note that the derivative w' must be discontinuous at the interface to guarantee the continuity of the axial stress.

In the forced vibration analysis, we will consider an axial traction applied at $x = 0$, shown in Fig. 3, and given by

$$p(t) = P \sin\left(\frac{\pi t}{T}\right) [\mathcal{H}(t) - \mathcal{H}(t - T)], \quad (34)$$

where \mathcal{H} is the Heaviside function, the dimension of P is force/area, and T measures the finite duration of the applied traction.

¹ The terms "right", and "left" are referred to the direction of the abscissa as shown in Fig. 2.

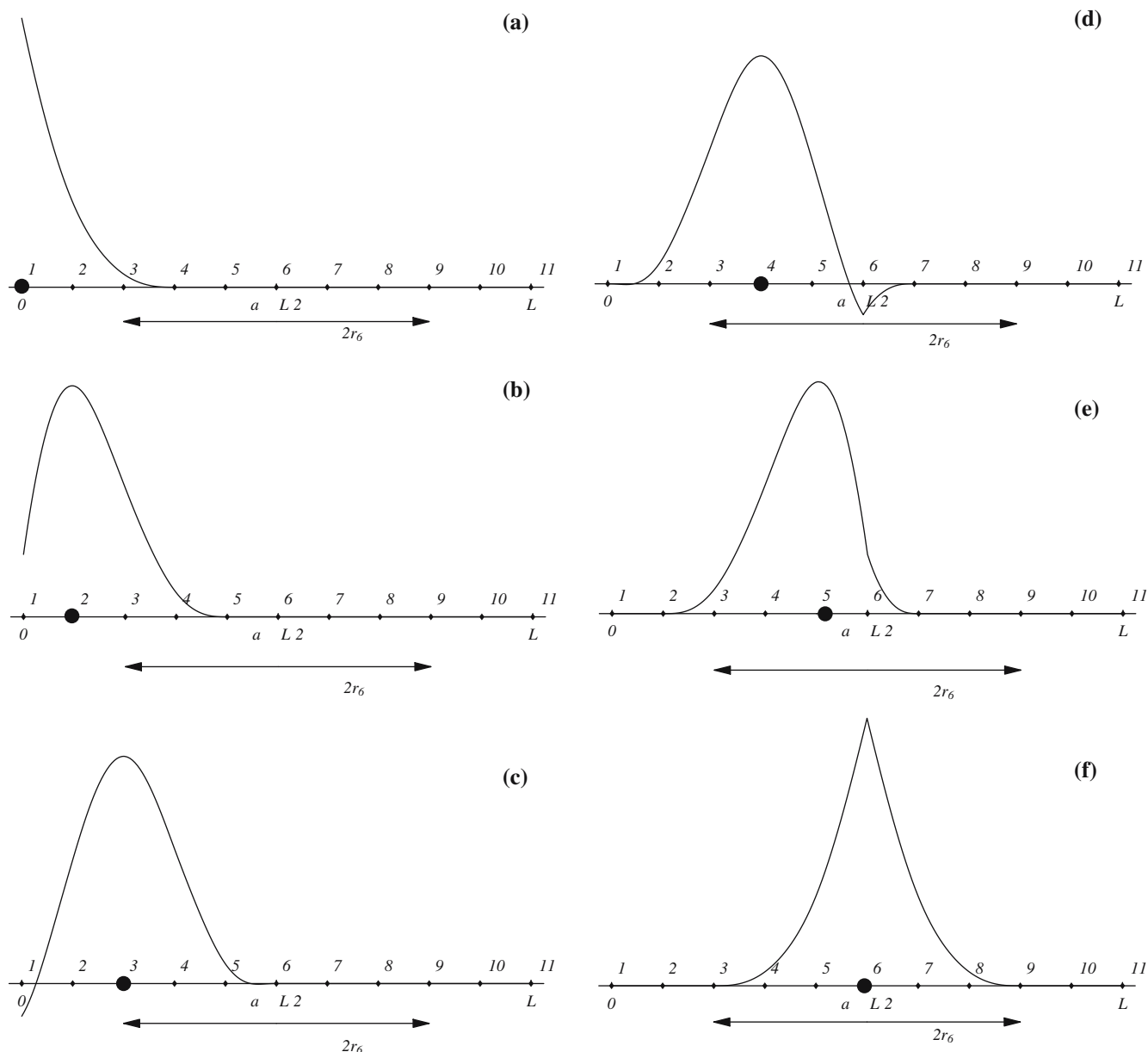


Fig. 1 Modified MLS basis functions for nodes 1 through 6 obtained with $m = 2$ and $r_i = 3L / (N - 1)$

3.2 MLPG6 weak and semidiscrete formulations

In this Section, the MLPG6 formulation of the boundary-value problem (26), (27), (28), (29), (30) and (31) is derived. A local symmetric augmented weak formulation (LSAWF) is stated for each one of the three methods of treating material discontinuities. The projection of trial and test functions on finite-dimensional basis functions leads to semidiscrete formulations of the problem, or equivalently a system of ordinary differential equations in time. It is shown that these mixed semidiscrete formulations are optimal, and stable in the sense that they satisfy both the ellipticity, and the inf-sup (Babuška-Brezzi) conditions.

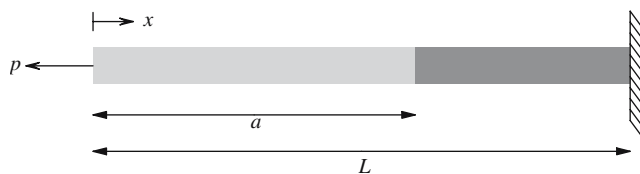


Fig. 2 Schematic sketch of the problem studied

3.2.1 Discontinuity modeled by a jump function

Semidiscrete formulation. Let $\Omega_S^i \subseteq [0, L], i = 1, 2, \dots, N$ be a family of subdomains of the global domain such that $\cup_{i=1}^N \Omega_S^i = [0, L]$. We introduce the following LSAWF of

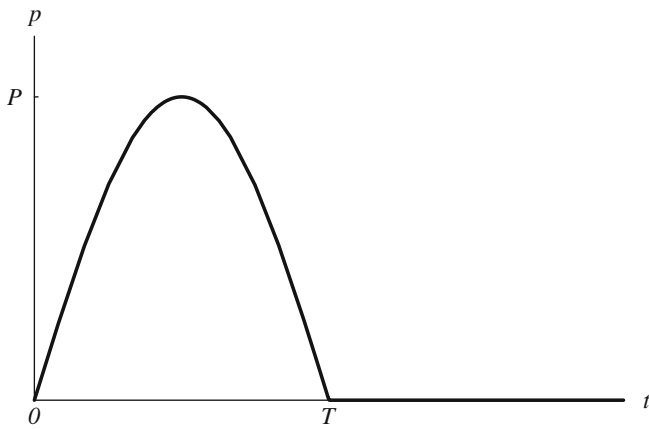


Fig. 3 Plot of the time-dependent axial traction applied at $x = 0$ the problem on the i -th subdomain Ω_S^i :

$$0 = \int_{\Omega_S^i} \rho \ddot{w} \tilde{w}_i dx + \int_{\Omega_S^i} E w' \tilde{w}_i' dx - [(1 - \delta_L) E w' \tilde{w}_i + \delta_L (\lambda_L \tilde{w}_i + \tilde{\lambda}_L w)]|_{\Gamma_S^{i+}} + [(1 - \delta_0) E w' \tilde{w}_i + \delta_0 p \tilde{w}_i]|_{\Gamma_S^{i-}}. \tag{35}$$

Here, $\tilde{w}_i \in H^1(0, L)$ is a test function for w ,

$$\delta_y(x) := \begin{cases} 1, & x = y \\ 0, & x \neq y \end{cases}, \tag{36}$$

and Γ_S^{i-} , Γ_S^{i+} are the left, and the right boundary points of the subdomain Ω_S^i . In order to enforce the essential boundary condition (31), the Lagrange multiplier λ_L has been introduced, and the scalar $\tilde{\lambda}_L$ is the corresponding test function. We emphasize that the natural boundary condition (28) has also been considered. The variational statement (35) can be derived by extremizing the Action related to an augmented Lagrangian on the set of isochronous motions following classical arguments, see e.g., Mura and Koya [24].

In order to capture the discontinuity in w' at the interface we enrich the smooth set of MLS basis functions $\psi(x)$ with a special jump function $\varkappa(x)$. Therefore, we approximate the axial displacement field by

$$w^h(x, t) = \psi^T(x) \widehat{\mathbf{w}}(t) + q(t) \varkappa(x), \tag{37}$$

where the additional unknown $q(t)$ represents the jump in the axial strain at time t . The jump function $\varkappa(x)$, and its first derivative are continuous in both segments of the bar, and its first derivative jumps at $x = a$ in order to ensure the continuity of the axial stress without affecting the continuity of the displacement field. Following Krongauz and Belytschko [17], we take

$$\varkappa(x) = \begin{cases} \frac{1}{6} - \frac{1}{2} \left(\frac{|x-a|}{r_J}\right) + \frac{1}{2} \left(\frac{|x-a|}{r_J}\right)^2 - \frac{1}{6} \left(\frac{|x-a|}{r_J}\right)^3, & \frac{|x-a|}{r_J} \leq 1 \\ 0, & \frac{|x-a|}{r_J} > 1 \end{cases}. \tag{38}$$

The size of the support of $\varkappa(x)$ equals $2r_J$ and, as shown in Fig. 4, the jump function and its derivative go to zero smoothly as $|x - a|/r_J \rightarrow 1$, while the derivative of $\varkappa\left(\frac{|x-a|}{r_J}\right)$ jumps from $1/2$ at $x = a^-$ to $-1/2$ at $x = a^+$.

In order to generate $N + 2$ equations for the $N + 1$ nodal unknowns

$$\widehat{\mathbf{u}}(t) = [\widehat{\mathbf{w}}(t) \ q(t)]^T, \tag{39}$$

and the Lagrange multiplier λ_L , we consider the set of $N + 2$ independent test functions

$$\Psi(x) = [\psi_1(x) \cdots \psi_N(x) \ \varkappa(x)]^T, \tag{40}$$

and $\tilde{\lambda}_L$. Thus an additional node is introduced at $x = a$. Setting the subdomain of integration to be the support of the i -th test function, and substituting into Eq. (35), the following semidiscrete local Bubnov–Galerkin (MLPG6) formulation arises:

$$\begin{cases} \mathbf{M} \ddot{\widehat{\mathbf{u}}}(t) + \mathbf{K} \widehat{\mathbf{u}}(t) + \mathbf{G} \lambda_L(t) = \mathbf{F}(t) \\ \mathbf{G}^T \widehat{\mathbf{u}}(t) = 0 \end{cases}. \tag{41}$$

Here,

$$[\mathbf{M}]_{ij} = \int_{\Omega_S^i} \rho \Psi_i \Psi_j dx, \quad [\mathbf{K}]_{ij} = \int_{\Omega_S^i} E \Psi_i' \Psi_j' dx, \tag{42}$$

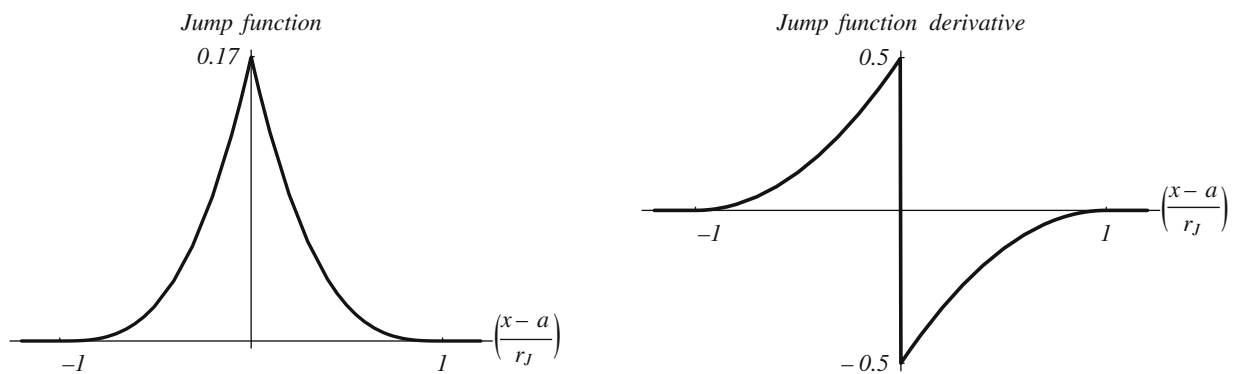


Fig. 4 Plots of the jump function $\varkappa\left(\frac{x-a}{r_J}\right)$, and its derivative

$$[\mathbf{F}(t)]_i = -\delta_0 p(t) \Psi_i|_{\Gamma_S^{i-}}, \quad i, j = 1, 2, \dots, N+1,$$

are the $(N+1) \times (N+1)$ mass, the stiffness, and the $(N+1) \times 1$ load matrices respectively, while the $(N+1) \times 1$ matrix \mathbf{G} appearing both in the equation of motion, and in the constraint equation is given by

$$[\mathbf{G}]_i = -\delta_L \Psi_i|_{\Gamma_S^{i+}}. \quad (43)$$

Inf-sup test. In order to achieve a stable, and optimal procedure for the MLPG6 method employing a Lagrange multiplier, the mixed formulation in static regimes should satisfy the ellipticity condition

$$\int_0^L E (w^{h'})^2 dx \geq \tilde{\alpha} \int_0^L (w^h)^2 dx, \quad \tilde{\alpha} > 0, \quad (44)$$

on the subspace H^{1N} of functions satisfying the homogeneous essential boundary condition (31). This ellipticity condition is satisfied because of Poincaré's inequality. Moreover, it should satisfy the inf-sup condition (see e.g., [5])

$$\inf_{\lambda_L \in \mathbb{R}/\{0\}} \sup_{w^h \in H^{1N}/\{0\}} \frac{\lambda_L w^h(L)}{\|\lambda_L\| \|w^h\|_{H^1}} \geq \tilde{\beta} > 0, \quad (45)$$

where $\|\lambda_L\| = |\lambda_L|$,

$$\|w\|_{H^1(0,L)}^2 := \int_0^L [w^2 + L^2 (w')^2] dx, \quad (46)$$

and $\tilde{\beta}$ is a constant independent of the nodal spacing. For $m = 1$, i.e., for complete monomial basis of order 0, the MLS basis functions reproduce exactly a constant function [see Eq. (4)], i.e., a rigid translation of the bar. Following Andreaus et al. [1] we choose, for any λ_L

$$w^h(x) = \lambda_L, \quad (47)$$

from which it follows that the inf-sup condition (45) is satisfied.

Reduced semidiscrete system of equations. Equation (41)₂ provides a constraint for the unknown vector $\hat{\mathbf{u}}$. By properly manipulating the system (41) we obtain a simpler formulation where the constraint is automatically satisfied.

Let $\ker \mathbf{G}^T$ be the null space of \mathbf{G}^T ; since the inf-sup condition holds, $\dim \ker \mathbf{G}^T = N$ (see e.g., [5]). Next, we introduce the $N \times (N+1)$ matrix \mathbf{X} whose rows constitute a basis for $\ker \mathbf{G}^T$, and the reduced N -vector of unknowns \mathbf{u} : $\hat{\mathbf{u}} = \mathbf{X}^T \mathbf{u}$. (48)

It is clear that the constraint equation is automatically satisfied for every $\mathbf{u} \in \mathbb{R}^N$. Substituting (48) into (41)₁, and premultiplying by \mathbf{X} one obtains the following reduced semidiscrete system of equations for \mathbf{u} :

$$\mathbf{m} \ddot{\mathbf{u}}(t) + \mathbf{k} \mathbf{u}(t) = \mathbf{f}(t), \quad (49)$$

where

$$\mathbf{m} = \mathbf{X} \mathbf{M} \mathbf{X}^T, \quad \mathbf{k} = \mathbf{X} \mathbf{K} \mathbf{X}^T, \quad \mathbf{f} = \mathbf{X} \mathbf{F}. \quad (50)$$

After solving for \mathbf{u} , we obtain the complete vector of unknowns $\hat{\mathbf{u}}$ by using Eq. (48).

3.2.2 Discontinuity modeled by modified MLS basis functions with discontinuous derivative

Let N nodes be located in the global domain $[0, L]$ with a node placed at the interface $x = a$, and let $\boldsymbol{\varphi}(x)$ be the set of MLS basis functions modified as in Sect. 2.2. The MLPG6 semidiscrete formulation is obtained in a similar way as for the method of jump function, i.e., by substituting in the LSAWF (35) the approximation $w^h(x, t) = \boldsymbol{\varphi}^T(x) \hat{\mathbf{w}}(t)$ for the trial solution, by considering the basis function φ_i as test function for the i -th subdomain, and by setting Ω_S^i equal to the support of φ_i . Therefore, the following $N+1$ equations for the N nodal unknowns $\hat{\mathbf{w}}$, and the Lagrange multiplier λ_L are obtained:

$$\begin{cases} \mathbf{M} \dot{\hat{\mathbf{w}}}(t) + \mathbf{K} \hat{\mathbf{w}}(t) + \mathbf{G} \lambda_L(t) = \mathbf{F}(t), \\ \mathbf{G}^T \hat{\mathbf{w}}(t) = 0. \end{cases} \quad (51)$$

The entries of the $(N \times N)$ mass and stiffness matrices, of the N load vector, and of the $(N \times 1)$ matrix \mathbf{G} are given by

$$[\mathbf{M}]_{ij} = \int_{\Omega_S^i} \varphi_i \varphi_j dx, \quad [\mathbf{K}]_{ij} = \int_{\Omega_S^i} E \varphi_i' \varphi_j' dx,$$

$$[\mathbf{F}(t)]_i = -\delta_0 p(t) \varphi_i|_{\Gamma_S^{i-}}, \quad (52)$$

$$[\mathbf{G}]_i = -\delta_L \varphi_i|_{\Gamma_S^{i+}}, \quad i, j = 1, 2, \dots, N. \quad (53)$$

It is easy to check (see Sect. 3.2.1) that the static form of the semidiscrete formulation (51) is elliptic, and that it satisfies the inf-sup condition. Therefore, we can introduce the reduced $(N-1)$ -vector of unknowns \mathbf{w} :

$$\hat{\mathbf{w}} = \mathbf{X}^T \mathbf{w}, \quad (54)$$

where \mathbf{X} is the $(N-1) \times N$ matrix whose rows constitute a basis for $\ker \mathbf{G}^T$. The constraint (51)₂ is then automatically satisfied; upon substitution into Eq. (51)₁, and premultiplication by \mathbf{X} one obtains a reduced system of $N-1$ equations for the $N-1$ unknowns \mathbf{w} formally analogous to (49).

3.2.3 Continuity of the displacement at the interface modeled by a Lagrange multiplier

Semidiscrete formulation. Let $\{x_i \in [0, a], i = 1, \dots, N_1\}$, $\{x_i \in [a, L], i = N_1 + 1, \dots, N_1 + N_2\}$ be two sets of nodes such that $x_{N_1} \equiv x_{N_1+1} = a$, and

$$\begin{aligned} \Omega_{S1}^i &\subset [0, a], \quad i = 1, \dots, N_1; \\ \Omega_{S2}^k &\subset [a, L], \quad k = N_1 + 1, N_1 + 2, \dots, N_1 \\ &\quad + N_2 - 1, N_1 + N_2 =: N, \end{aligned} \quad (55)$$

be the corresponding disjoint families of subdomains covering $[0, a]$, and $[a, L]$, respectively. Following Cordes and

Moran [11], we consider the augmented variational statement

$$\begin{aligned}
0 = & \int_{\Omega_{S1}^i} \varrho_1 \ddot{w}_1 \tilde{w}_{1i} dx + \int_{\Omega_{S1}^i} E_1 w_1' \tilde{w}_{1i}' dx \\
& + \int_{\Omega_{S2}^k} \varrho_2 \ddot{w}_2 \tilde{w}_{2k} dx + \int_{\Omega_{S2}^k} E_2 w_2' \tilde{w}_{2k}' dx \quad (56) \\
& - [(1 - \delta_a) E_1 w_1' \tilde{w}_{1i} - \delta_a (\lambda_a \tilde{w}_{1i} + \tilde{\lambda}_a w_1)]|_{\Gamma_{S1}^{i+}} \\
& + [(1 - \delta_0) E_1 w_1' \tilde{w}_{1i} + \delta_0 p \tilde{w}_{1i}]|_{\Gamma_{S1}^{i-}} \\
& - [(1 - \delta_L) E_2 w_2' \tilde{w}_{2k} + \delta_L (\lambda_L \tilde{w}_{2k} + \tilde{\lambda}_L w_2)]|_{\Gamma_{S2}^{k+}} \\
& + [(1 - \delta_a) E_2 w_2' \tilde{w}_{2k} - \delta_a (\lambda_a \tilde{w}_{2k} + \tilde{\lambda}_a w_2)]|_{\Gamma_{S2}^{k-}}.
\end{aligned}$$

Here, \tilde{w}_{1i} , \tilde{w}_{2k} , $\tilde{\lambda}_a$, and $\tilde{\lambda}_L$ are test functions for the displacement fields, and the Lagrange multipliers λ_a and λ_L , introduced to enforce the continuity of the displacement at the interface (29), and the essential boundary condition (31). We emphasize that, in this approach, two problems are separately formulated in the two homogenous parts of the bar; two overlapping nodes are placed at the interface, and the two problems are connected by the Lagrange multiplier λ_a . Note that the natural boundary condition (30) is taken into account only in the weak sense.

The MLPG6 semidiscrete formulation is derived by substituting into the LSAWF (56) the global approximations for the trial solutions:

$$w_1^h(x, t) = \boldsymbol{\psi}_1(x)^T \hat{\mathbf{w}}_1(t), \quad w_2^h(x, t) = \boldsymbol{\psi}_2(x)^T \hat{\mathbf{w}}_2(t), \quad (57)$$

where $\boldsymbol{\psi}_1(x)$, and $\boldsymbol{\psi}_2(x)$ are the MLS basis functions defined separately in domains $[0, a]$, and $[a, L]$. Furthermore the MLS basis function $\psi_{\alpha i}$ ($\alpha = 1, 2$) are taken as the test function in the subdomain $\Omega_{S\alpha}^i$ ($\alpha = 1, 2$) with support equal to that of the corresponding MLS basis function. Therefore, the system of $(N + 2)$ ODEs

$$\begin{cases} \mathbf{M} \ddot{\hat{\mathbf{w}}}(t) + \mathbf{K} \hat{\mathbf{w}}(t) + \mathbf{G} \boldsymbol{\Lambda}(t) = \mathbf{F}(t) \\ \mathbf{G}^T \hat{\mathbf{w}}(t) = \mathbf{0} \end{cases}, \quad N = N_1 + N_2, \quad (58)$$

for the $(N + 2)$ unknowns

$$\hat{\mathbf{w}} = [\hat{\mathbf{w}}_1 \ \hat{\mathbf{w}}_2]^T, \quad \boldsymbol{\Lambda} = [\lambda_a \ \lambda_L]^T, \quad (59)$$

is obtained. In Eq. (58), \mathbf{M} , \mathbf{K} , and \mathbf{F} are, respectively, the $(N \times N)$ mass, the $(N \times N)$ stiffness, and the $N \times 1$ load matrices:

$$\mathbf{M} = \begin{bmatrix} \mathbf{M}_1 & \mathbf{0} \\ \mathbf{0} & \mathbf{M}_2 \end{bmatrix}, \quad \mathbf{K} = \begin{bmatrix} \mathbf{K}_1 & \mathbf{0} \\ \mathbf{0} & \mathbf{K}_2 \end{bmatrix}, \quad \mathbf{F} = \begin{bmatrix} \mathbf{F}_1 \\ \mathbf{0} \end{bmatrix}, \quad (60)$$

with

$$\begin{aligned}
[\mathbf{M}_\alpha]_{ij} &= \int_{\Omega_{S\alpha}^i} \varrho_\alpha \psi_{\alpha i} \psi_{\alpha j} dx, \quad [\mathbf{K}_\alpha]_{ij} = \int_{\Omega_{S\alpha}^i} E_\alpha \psi_{\alpha i}' \psi_{\alpha j}' dx, \\
[\mathbf{F}_1]_i &= -p \delta_0 \left(\Gamma_{S1}^{i-} \right) \psi_{1i} \left(\Gamma_{S1}^{i-} \right), \\
\alpha &= 1, 2, \quad i, j = 1, 2, \dots, N_\alpha. \quad (61)
\end{aligned}$$

The $(N \times 2)$ matrix

$$\mathbf{G} = \begin{bmatrix} \mathbf{G}_{1\lambda_a} & \mathbf{0} \\ \mathbf{G}_{2\lambda_a} & \mathbf{G}_{2\lambda_L} \end{bmatrix}, \quad (62)$$

is defined by

$$\begin{aligned}
[\mathbf{G}_{1\lambda_a}]_i &= \delta_a \left(\Gamma_{S1}^{i+} \right) \psi_{1i} \left(\Gamma_{S1}^{i+} \right), \\
[\mathbf{G}_{2\lambda_a}]_k &= -\delta_a \left(\Gamma_{S2}^{i-} \right) \psi_{2i} \left(\Gamma_{S2}^{i-} \right), \\
[\mathbf{G}_{2\lambda_L}]_k &= -\delta_L \left(\Gamma_{S2}^{i+} \right) \psi_{2i} \left(\Gamma_{S2}^{i+} \right), \\
i &= 1, \dots, N_1, \quad k = 1, \dots, N_2. \quad (63)
\end{aligned}$$

Inf-sup test. For the static version of this linear problem, the ellipticity condition is readily satisfied. More effort is needed to show that the mixed formulation in static regimes satisfies the inf-sup condition as well, that is

$$\begin{aligned}
\inf_{\boldsymbol{\Lambda} \in \mathbb{R}^{2/\{0\}}} \sup_{w^h \in W^h/\{0\}} \frac{\lambda_a (w_2^h(a) - w_1^h(a)) + \lambda_L w_2^h(L)}{\|\boldsymbol{\Lambda}\| \|w^h\|_{W^h}} \\
\geq \tilde{\beta} > 0, \quad (64)
\end{aligned}$$

where $\tilde{\beta}$ is a constant independent of the nodal spacing, $W^h \subset H^1(0, a) \times H^1(a, L)$ is the N -dimensional MLS solution space, $\|\boldsymbol{\Lambda}\|^2 = \boldsymbol{\Lambda}^T \boldsymbol{\Lambda}$, and

$$\begin{aligned}
\|w^h\|_{W^h}^2 &:= \int_0^a \left[(w_1^h)^2 + L^2 (w_1^h)'^2 \right] dx \\
&+ \int_a^L \left[(w_2^h)^2 + L^2 (w_2^h)'^2 \right] dx, \quad (65)
\end{aligned}$$

is the W^h norm. From Eq. (4) it is clear that the MLS basis functions with $m = 1$ exactly reproduce a constant function. Therefore, for any given $\boldsymbol{\Lambda}$ we choose

$$w_1^h(x) = \lambda_L - \lambda_a, \quad w_2^h(x) = \lambda_L. \quad (66)$$

Hence

$$\begin{aligned}
\lambda_a \left(w_2^h(a) - w_1^h(a) \right) + \lambda_L w_2^h(L) &= \|\boldsymbol{\Lambda}\|^2, \\
\|w^h\|_{W^h}^2 &= \boldsymbol{\Lambda}^T \mathbf{S} \boldsymbol{\Lambda}, \quad (67)
\end{aligned}$$

where \mathbf{S} is the following symmetric positive-definite matrix:

$$\mathbf{S} = \begin{bmatrix} a & -a \\ -a & L \end{bmatrix}. \quad (68)$$

From Eq. (67) we can establish that

$$\mu_1 \|\boldsymbol{\Lambda}\|^2 \leq \|w^h\|_{W^h}^2 \leq \mu_2 \|\boldsymbol{\Lambda}\|^2, \quad (69)$$

where

$$\begin{aligned}
\mu_1 &= \frac{1}{2} \left(a + L - \sqrt{(L - a)^2 + 4a^2} \right), \\
\mu_2 &= \frac{1}{2} \left(a + L + \sqrt{(L - a)^2 + 4a^2} \right), \quad (70)
\end{aligned}$$

are eigenvalues of \mathbf{S} . Since

$$\frac{\lambda_a (w_2^h(a) - w_1^h(a)) + \lambda_L w_2^h(L)}{\|\mathbf{\Lambda}\| \|w^h\|_{W^h}} = \sqrt{\frac{\mathbf{\Lambda}^T \mathbf{\Lambda}}{\mathbf{\Lambda}^T \mathbf{S} \mathbf{\Lambda}}}, \quad (71)$$

we have

$$\sup_{w^h \in W^h/\{0\}} \frac{\lambda_a (w_2^h(a) - w_1^h(a)) + \lambda_L w_2^h(L)}{\|\mathbf{\Lambda}\| \|w^h\|_{W^h}} \geq \sqrt{\frac{\mathbf{\Lambda}^T \mathbf{\Lambda}}{\mathbf{\Lambda}^T \mathbf{S} \mathbf{\Lambda}}}, \quad (72)$$

which implies that

$$\begin{aligned} & \inf_{\mathbf{\Lambda} \in \mathbb{R}^2/\{0\}} \sup_{w^h \in W^h/\{0\}} \frac{\lambda_a (w_2^h(a) - w_1^h(a)) + \lambda_L w_2^h(L)}{\|\mathbf{\Lambda}\| \|w^h\|_{W^h}} \\ & \geq \inf_{\mathbf{\Lambda} \in \mathbb{R}^2} \sqrt{\frac{\mathbf{\Lambda}^T \mathbf{\Lambda}}{\mathbf{\Lambda}^T \mathbf{S} \mathbf{\Lambda}}} = \frac{1}{\sqrt{\mu_2}}. \end{aligned} \quad (73)$$

Thus the inf-sup condition is satisfied since μ_2 depends only on a and L , and is independent of the nodal spacing.

Reduced semidiscrete system of equations. Let $\ker \mathbf{G}^T$ be the null space of \mathbf{G}^T ; since the inf-sup condition holds, we have $\dim \ker \mathbf{G}^T = N - 2$. Next, let rows of the $(N - 2 \times N)$ matrix \mathbf{X} be comprised of $(N - 2)$ linearly independent vectors in $\ker \mathbf{G}^T$, and let us introduce the $(N - 2)$ reduced vector of unknowns \mathbf{w} :

$$\widehat{\mathbf{w}} = \mathbf{X}^T \mathbf{w}. \quad (74)$$

In this way, the constraint Eq. (58)₂ is automatically satisfied for every $\mathbf{w} \in \mathbb{R}^{(N-2)}$. Upon substitution into Eq. (58)₁, and premultiplication by \mathbf{X} one obtains the reduced semidiscrete system of $N - 2$ equations:

$$\mathbf{m} \ddot{\mathbf{w}} + \mathbf{k} \mathbf{w} = \mathbf{f}, \quad (75)$$

where the $(N - 2 \times N - 2)$ reduced mass and stiffness matrices, and the reduced $(N - 2)$ load vector are defined as in Eq. (50).

3.3 Time integration scheme

We integrate the reduced semidiscrete system of equations with initial conditions

$$\begin{aligned} \mathbf{w}(0) &= \mathbf{0}, \\ \dot{\mathbf{w}}(0) &= \mathbf{0}, \end{aligned} \quad (76)$$

with the Newmark family of methods [14], and get

$$\begin{aligned} \mathbf{m} \mathbf{a}_{n+1} + \mathbf{k} \mathbf{w}_{n+1} &= \mathbf{f}_{n+1}, \\ \mathbf{w}_{n+1} &= \mathbf{w}_n + \Delta t \mathbf{v}_n \\ &+ \frac{\Delta t^2}{2} [(1 - 2\beta) \mathbf{a}_n + 2\beta \mathbf{a}_{n+1}], \quad (77) \\ \mathbf{v}_{n+1} &= \mathbf{v}_n + \Delta t [(1 - \gamma) \mathbf{a}_n + \gamma \mathbf{a}_{n+1}], \end{aligned}$$

where \mathbf{a}_n , \mathbf{v}_n , and \mathbf{w}_n are approximations of $\ddot{\mathbf{w}}(t_n)$, $\dot{\mathbf{w}}(t_n)$, and $\mathbf{w}(t_n)$, respectively, $\mathbf{f}_{n+1} = \mathbf{f}(t_{n+1})$, Δt is the time step, and β and γ are parameters.

Depending upon the choice of β and γ , different members of the Newmark family arise. Gu and Liu [13], in the analysis of forced vibrations of homogeneous bodies, compared the performances of the explicit and conditionally stable central difference method ($\beta = 0$, $\gamma = 1/2$), and the implicit and unconditionally stable average acceleration ($\beta = 1/4$, $\gamma = 1/2$) method. They showed that the average acceleration method gives very good results with larger time steps than those allowed by the central difference method. Qian and Batra [29] employed the central-difference method to integrate the coupled ordinary differential equations derived by the MLPG approximation of the transient thermoelastic problem for a functionally graded material.

Here we also use these two methods, both the consistent, and the lumped mass matrices, and for the average acceleration method set

$$\Delta t = 10^{-2} T, \quad T = \frac{2}{5} \tau, \quad \tau := \frac{a}{c_1} + \frac{L - a}{c_2}, \quad (78)$$

$$c_1 = \sqrt{\frac{E_1}{\rho_1}}, \quad c_2 = \sqrt{\frac{E_2}{\rho_2}},$$

where τ is the time when the wave is reflected at the clamped end, and c_1 and c_2 are wave speeds in the two materials. For values assigned to material parameters the first reflection of the wave occurs at the clamped end.

3.4 Numerical evaluation of domain integrals

Since the MLS basis functions are not polynomials, it is difficult to integrate accurately the discrete local weak forms associated with the MLPG6 formulation, and obtain the mass, and the stiffness matrices.

We adopt the integration procedure proposed by Atluri et al. [4]. The idea is sketched in Fig. 5, where a possible arrangement of nodes is shown. The integration on Ω_S^i is performed by carrying out the integration on each subregion, obtained by dividing Ω_S^i by boundaries of subdomains of other nodes in the neighborhood of node i . With this method, integrals are evaluated with five quadrature points in each intersected region.

4 Numerical results and comparisons

4.1 Values of parameters

Results have been computed for following values of the material parameters

$$\begin{aligned} \rho_1 &= 7,860 \text{ kg/m}^3, & E_1 &= 200 \text{ GPa}, \\ \rho_2 &= 2,710 \text{ kg/m}^3, & E_2 &= 70 \text{ GPa}, \end{aligned} \quad (79)$$

corresponding to steel (material “1”) and aluminum (material “2”). The geometry is defined by

$$L = 50 \text{ mm}, \quad a = L/2 = 25 \text{ mm}. \quad (80)$$

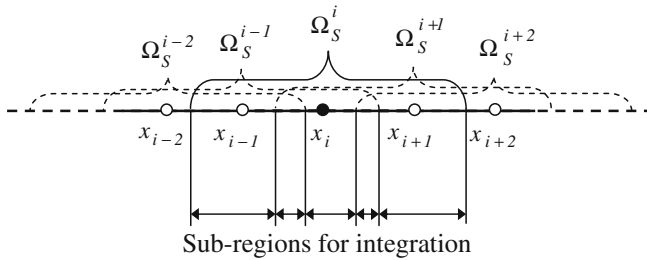


Fig. 5 Subdomain Ω_S^i of node x_i , and integration subregions obtained by the intersection of Ω_S^i with supports of domains of influence of neighboring nodes

For these values we have

$$\tau = 9.87 \mu s, \quad T = 3.95 \mu s. \tag{81}$$

The numerical value of P has been chosen as

$$P = 100 \text{ MPa}. \tag{82}$$

The MLS basis functions are generated by complete monomials of degree 1. Except when we discuss convergence of the solution with an increase in the number of uniformly spaced nodes, results presented below have been computed with 81 uniformly spaced nodes. When we model the discontinuity with either the jump function or the modified MLS basis functions the domain $[0, L]$ is discretized with equally spaced nodes with one node placed at the interface. In both cases the semi-support r_i of the weight function W_i is

$$r_i = \begin{cases} 2 \frac{L}{N-1}, & i = 2, 3, \dots, N-1 \\ 4 \frac{L}{N-1}, & i = 1, N \end{cases}; \tag{83}$$

and for the modified MLS basis functions the semi-support of the weight function for the node at the interface is set equal to $4L/(N-1)$.

When using a Lagrange multiplier to enforce the continuity of displacements at $x = a$, an equal number of uniformly spaced nodes is used in the domains $[0, a]$ and $[a, L]$, and Eq. (83) holds in each homogeneous part of the bar with L equal to the segment length and N equal to the total number of nodes in the segment.

From numerical experiments it has been found that the choice of the radius r_J of the jump function support strongly affects the accuracy of computed results. Here we take

$$r_J = \frac{N}{2} \frac{L}{N-1}; \tag{84}$$

thus one-half of nodes used in the discretization are included in the jump function semisupport.

4.2 Convergence analysis

For each of the three methods of accounting for the material discontinuity at $x = a$, convergence tests are performed for both the solution of a static problem, and mode shapes of the bimaterial clamped bar. Two relative error norms are used for this purpose:

- Relative L^2 error norm

$$\sqrt{\frac{\int_0^L (w^h - w^e)^2 dx}{\int_0^L (w^e)^2 dx}}; \tag{85}$$

- Relative H^1 error norm

$$\sqrt{\frac{\int_0^L \left((w^h - w^e)^2 + L^2 \left((w^h)' - (w^e)' \right)^2 \right) dx}{\int_0^L \left((w^e)^2 + L^2 \left((w^e)' \right)^2 \right) dx}}; \tag{86}$$

where superscripts h and e refer to the MLPG6 numerical solution, and the analytical solution respectively. For the static deformation with constant uniformly distributed load P/L , Fig. 6 shows variations of the relative L^2 and H^1 error norms with an increase in the number of nodes obtained with, and without employing one of the three techniques to account for the material discontinuity at $x = a$. Results have also been computed with the FEM with piecewise linear basis functions, and a node placed at the interface. In this and other Figures, notations J, L, and MMLS signify, respectively, results obtained with the methods of jump function, the Lagrange multipliers, and the modified MLS basis functions. The plots reveal the monotonic convergence of the MLPG solution; the error without treatment of the material discontinuity, denoted by the curve marked MLS, is higher than that with the FEM, with convergence rates of 1 (0.5)

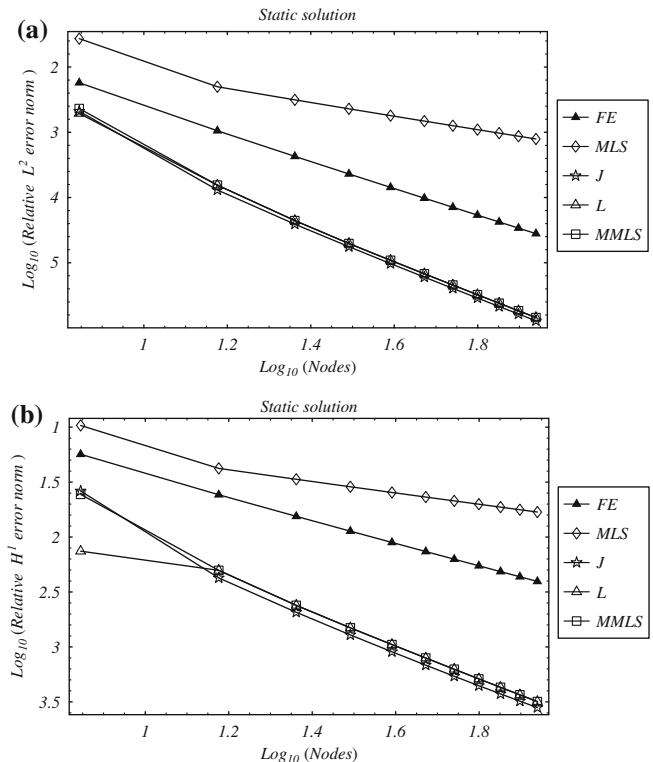


Fig. 6 a Relative L^2 error norm and, **b** relative H^1 error norm for static deformations under uniformly distributed load along the length of the bar

and 2 (1), respectively, in the L^2 (H^1) norm. When a special technique is used to treat the material discontinuity, the error in the MLPG solution is always lower than that with the FEM and the MLPG solution converges faster to the analytical one, at approximate rates of 2.5 and 1.5 respectively in the L^2 and H^1 norms. The need for treating the material discontinuity is evident from examining Fig. 7a, where the axial displacement derivative near the interface computed with and without the use of these special methods is depicted. A treatment of discontinuity is necessary in order to accurately model the jump in the displacement gradient at the interface $x = a$; however, the displacement gradient computed away from $x = a$ without employing any one of the three methods is close to the analytical one. We have plotted the percentage error in the four numerical solutions in Fig. 7b, c. It is evident that without using a method to account for the discontinuity in the displacement gradient at $x = a$, the error in the computed solution exceeds 50%. However, when any one of the three methods is used to consider the material discontinuity, then the maximum error in the displacement gradient is less than 0.5%.

The numerical eigenfrequencies, and mode shapes are obtained by searching for solutions of the type

$$\mathbf{w}(t) = \underline{\mathbf{w}} \exp(i\omega t), \quad (87)$$

of the reduced semidiscrete system of equations, and discarding the applied loads. Therefore, the following eigenvalue problem arises:

$$(\mathbf{k} - \omega^2 \mathbf{m}) \underline{\mathbf{w}} = \mathbf{0}. \quad (88)$$

In Fig. 8, we report the relative L^2 and H^1 error norms of the first three mode shapes; the mode shapes are shown in Fig. 9. As before, the MLPG6 solution without treatment of the material discontinuity gives higher errors than the MLPG6 solutions obtained by modeling the material discontinuity with any one of the three techniques. In both the L^2 and the H^1 norms, whereas the rate of convergence of the numerical solution without treatment of material discontinuity is lower than that of the FE solution, the MLPG6 solutions with the material discontinuity treatment converge faster. For the first three modes, the convergence rates in the L^2 norm with and without treatment of discontinuity are 2.5 and 1.5, respectively, against a convergence rate of 2 for the FEM. In the H^1 norm, the corresponding convergence rates are 1.5, 0.5, and 1, respectively.

In Fig. 10 the relative errors in the first two eigenfrequencies are reported; the analytically computed first two eigenfrequencies are 0.108 and 0.528 MHz. In both cases, the convergence rates are 3 and 1 for the MLPG6 solutions with, and without the treatment of material discontinuity respectively, and 2 for the FE solution. Furthermore, frequencies converge monotonically from above to their analytical values. For the MLPG1 formulation of plate-theory equations, Qian et al. [28] found that the first four flexural frequencies did not converge from above with an increase in the number of nodes.

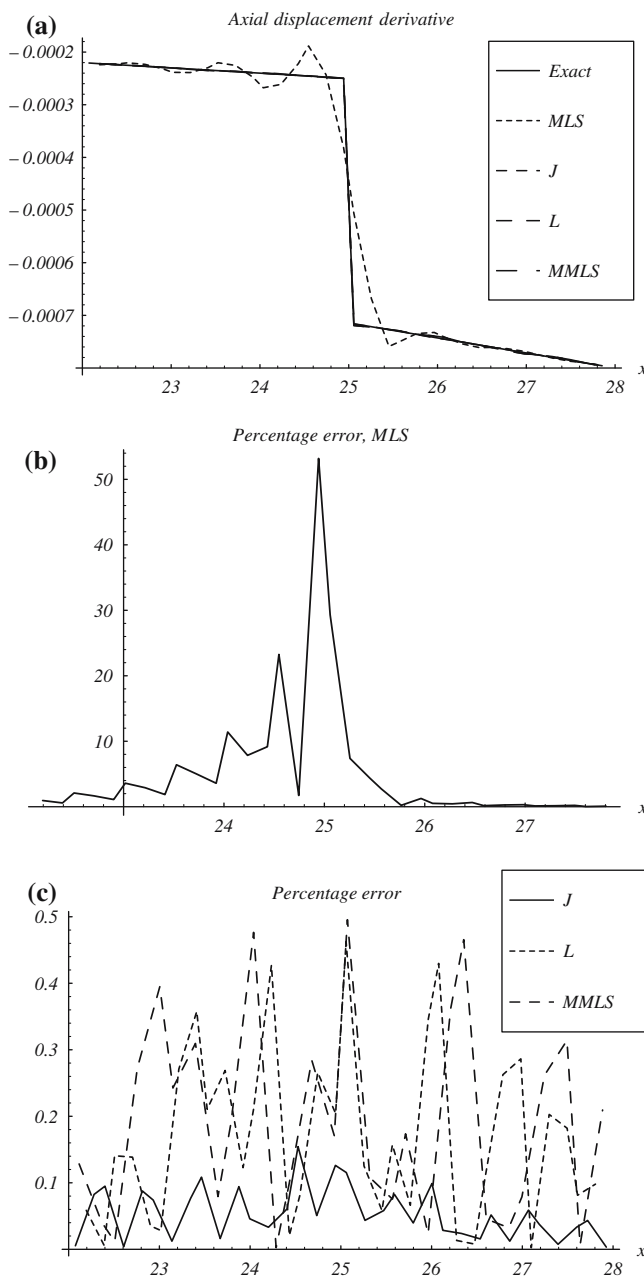


Fig. 7 a Axial displacement gradient near the material interface for a static deformation, and b, c the percentage error in the derivative of the static solution for the uniformly distributed load, P/L , obtained with the MLS basis functions without treatment of the material discontinuity; the MLS basis functions with the three methods of treating the material discontinuity

4.3 Forced vibrations

The MLPG solutions have been computed by using uniformly spaced 81 nodes on the global domain.

In Fig. 11 we report two snapshots of the traveling stress wave computed with the average acceleration method at

$$t_1 = \frac{a}{c_1} + \frac{3T}{4} \simeq 7.9 \mu\text{s}, \quad t_2 = \tau + 2T \simeq 17.7 \mu\text{s}, \quad (89)$$

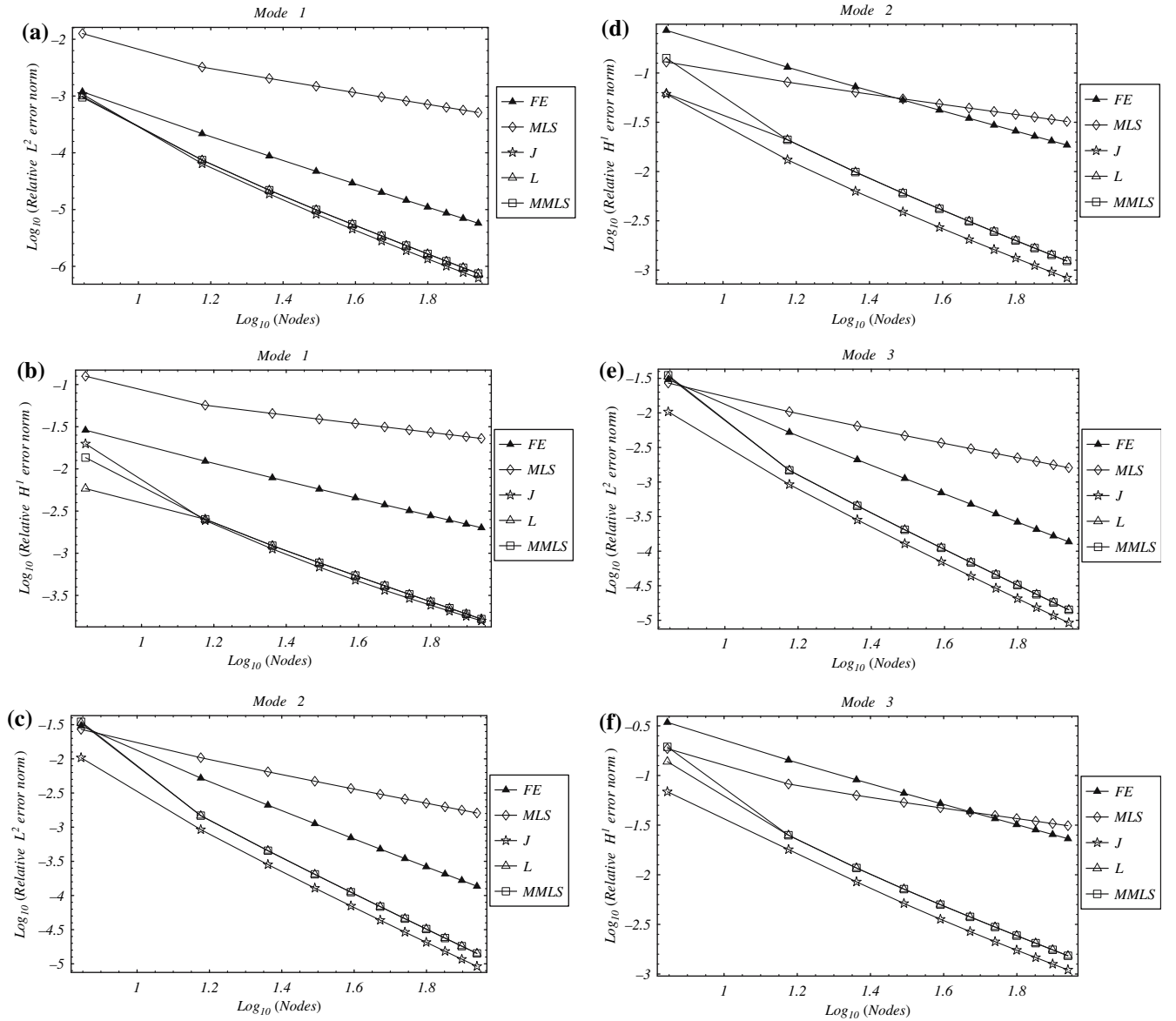


Fig. 8 Relative L^2 and H^1 error norms for the first three mode shapes

and in Fig. 12 we show the axial displacement at the same instants. Times t_1 and t_2 are, respectively, the instants when three-fourth of the wave has crossed the interface $x = a$ between the two materials, and when the two waves reflected from the free, and the clamped edges overlap at $x = a$. Comparisons have been made with analytical solutions obtained by setting $j = 3$ in summations (109), and (110), since for this value of j

$$\max_{t \in \{t_1, t_2\}} \left(\int_0^L (w^e(x, t)|_{j+1} - w^e(x, t)|_j)^2 dx \right) \leq 10^{-15} L^3, \quad (90)$$

where $w^e(x, t)|_j$ is the analytical solution [Eqs. (109), (110)] computed for a given value of j . The good agreement with the analytical results shows that all three methods for the treatment of material discontinuity are able to capture well both the reflection of, and the interaction among propagating waves; the numerical solutions virtually overlap the analytic solution.

In Fig. 13a–d we depict the time history of the axial displacement at the left end computed with the central difference method by using both the consistent, and the lumped mass matrices, with $\Delta t = 0.9\Delta t_{\text{cr}}$ and $1.01\Delta t_{\text{cr}}$, respectively. The critical time step is given by

$$\Delta t_{\text{cr}} = \frac{2}{\max(\omega_i^h)}. \quad (91)$$

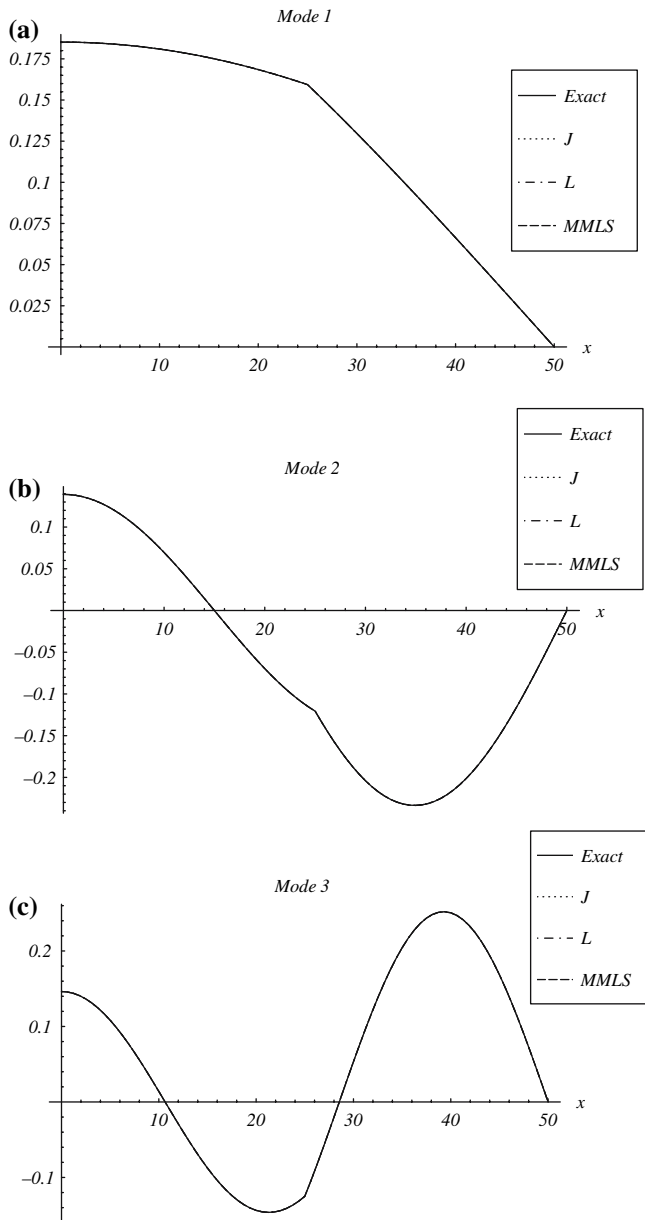


Fig. 9 First three mode shapes of the segmented bar

Table 1 Critical time step, Δt_{cr} [μs], for different methods of accounting for material discontinuity

	Mass matrix	
	Consistent	Lumped
Jump function	0.0393	0.204
Lagrange multiplier	0.0671	0.203
Modified MLS	0.0671	0.203

Here ω_i^h is i -th natural eigenfrequency of the system. Values of Δt_{cr} for the consistent, and the lumped mass matrices, and the three methods of accounting for the material discontinuity are listed in Table 1. Comparisons are made with analytical solutions obtained by summing up to $j = 7$ in Eqs. (109), (110), since for this value of j

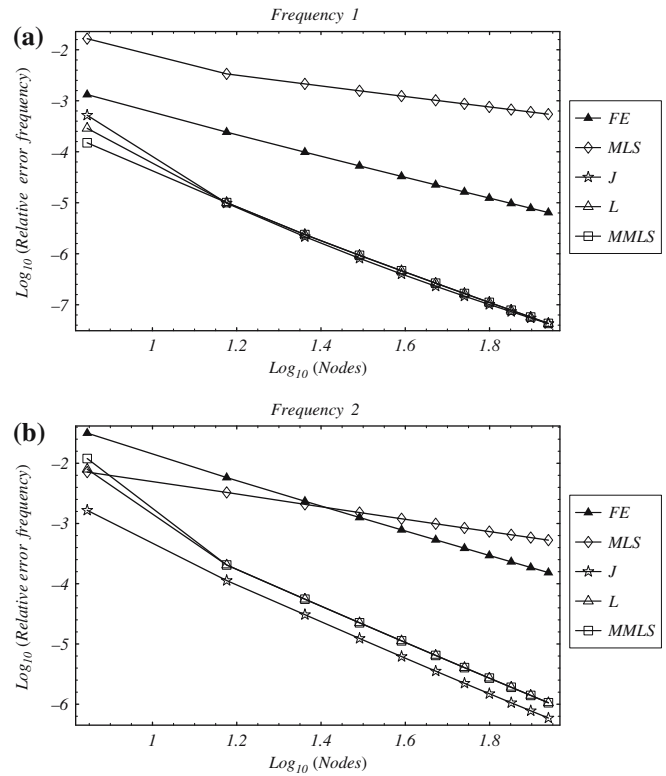


Fig. 10 Relative error in the estimation of the first two natural frequencies

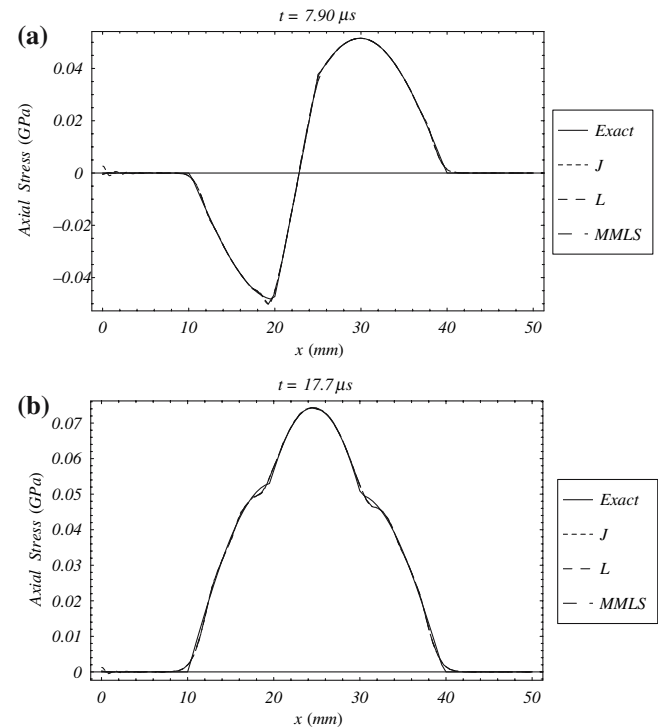


Fig. 11 Snapshots of the traveling stress wave at a $t = \frac{a}{c_1} + \frac{3T}{4}$ and b $t = \tau + 2T$

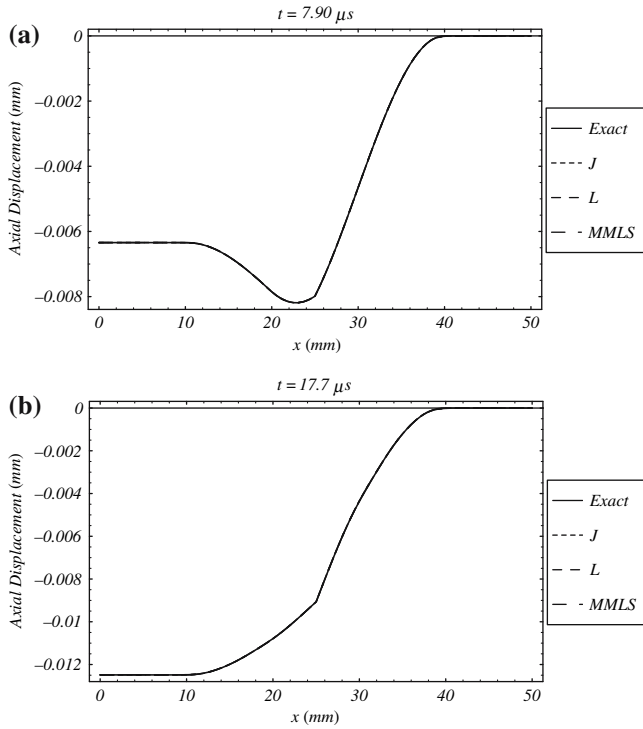


Fig. 12 Snapshots of the displacement wave at **a** $t = \frac{a}{c_1} + \frac{3T}{4}$ and **b** $t = \tau + 2T$

$$\int_0^{\bar{t}} \left(w^e(0, t)|_{j+1} - w^e(0, t)|_j \right)^2 dt \leq 10^{-15} L^2 \bar{t}, \quad (92)$$

where $w^e(x, t)|_j$ is the analytical solution [Eqs. (109), (110)] computed for a given value of j , and $\bar{t} = 8(a/c_1 + (L - a)/c_2)$ is the maximum time considered in the computations.

Whereas for the lumped mass matrix obtained by the row sum technique Δt_{cr} has the same value for the three methods of accounting for the material discontinuity, it is not so for the consistent mass matrix; Δt_{cr} for the method of jump function is nearly one-half of that for the other two methods. A possible explanation is that the jump function technique modifies the basis functions and the consistent mass matrix unfavorably for the maximum eigenfrequency of the system. However, when the lumped mass matrix is obtained by the row sum technique, the effect of the modification of basis functions is eliminated, and the maximum natural frequency is the same for the three methods.

Solutions obtained with the three methods of accounting for the material discontinuity essentially coincide with the analytical solution of the problem. Results plotted in Fig. 13a–d signify the well known fact that the solution computed with $\Delta t < \Delta t_{cr}$ is stable, and that with $\Delta t > \Delta t_{cr}$ is unstable. A comparison of plots of Figs. 13a, c reveals that the consistent mass matrix gives lower errors than the lumped mass matrix.

For the average acceleration method, only the consistent mass matrix is considered. Figure 13e–f exhibit the well

known fact that the average acceleration algorithm is unconditionally stable, as evidenced by the stability of the solution even when the time step size equals $1.5\Delta t_{cr}^{consistent}$, and $1.5\Delta t_{cr}^{lumped} \sim 0.3 \mu s$.

In Fig. 14 we report the time history of the jump

$$\left| \sigma^h(a^+, t) - \sigma^h(a^-, t) \right|, \quad (93)$$

in the axial stress at the interface computed by using the method of (a) the jump function, (b) the Lagrange multiplier, and (c) the modified MLS basis functions. Ideally it should be zero for all times. As we can see, the method (a) is the most accurate; this is because it models both the displacement continuity, and the axial stress continuity at $x = a$, while with the other two techniques the essential boundary condition (29) is directly enforced but the axial stress continuity (30) is weakly satisfied.

For the average acceleration method, and the consistent mass matrix, Fig. 15 exhibits the effect of decreasing the time step size on the L^2 error norm of the axial stress at times $7.91 \mu s$ and $17.8 \mu s$. The MLPG method with one of the three methods of considering the material discontinuity gives lower errors than the FEM.

Batra et al. [8], and Qian and Batra [29] have compared the MLPG and the FE formulations for transient problems.

5 Conclusions

We have used the meshless local Bubnov–Galerkin (MLPG6) method to study free, and forced vibrations of a segmented bar comprised of two materials. Because of the higher-order differentiability of the MLS basis functions, special techniques are needed to accurately model jumps in displacement gradients at the material interfaces. Here, we have employed methods of (a) the jump function, (b) the Lagrange multiplier, and (c) the modified MLS basis functions with discontinuous derivative. In all cases the essential boundary condition has been enforced by introducing a Lagrange multiplier.

The stability of methods has been assessed by analytically proving the inf-sup condition. Reduced semidiscrete systems are derived, where constraints are automatically satisfied. The direct analysis of forced vibrations is performed by using the β -Newmark family of methods, and the spatial integration in the MLPG formulation uses Gauss quadrature rules. Both the lumped, and the consistent mass matrices with the central-difference method are used, while only consistent mass matrix with the average acceleration method is considered.

Numerical results for a bimaterial bar, clamped at one end, and free at the other end, computed with the MLPG6 formulations have been compared with those obtained with the FEM, and analytically. Both for static, and dynamic problems studied, convergence rates of the MLPG6 solution without any treatment of material discontinuities are lower than those of the FE solution. However, when any one of the three techniques to account for the material discontinuity is used, the MLPG6 solution converges faster than the FE solution. For a fixed number of nodes, errors in the MLPG6 solution

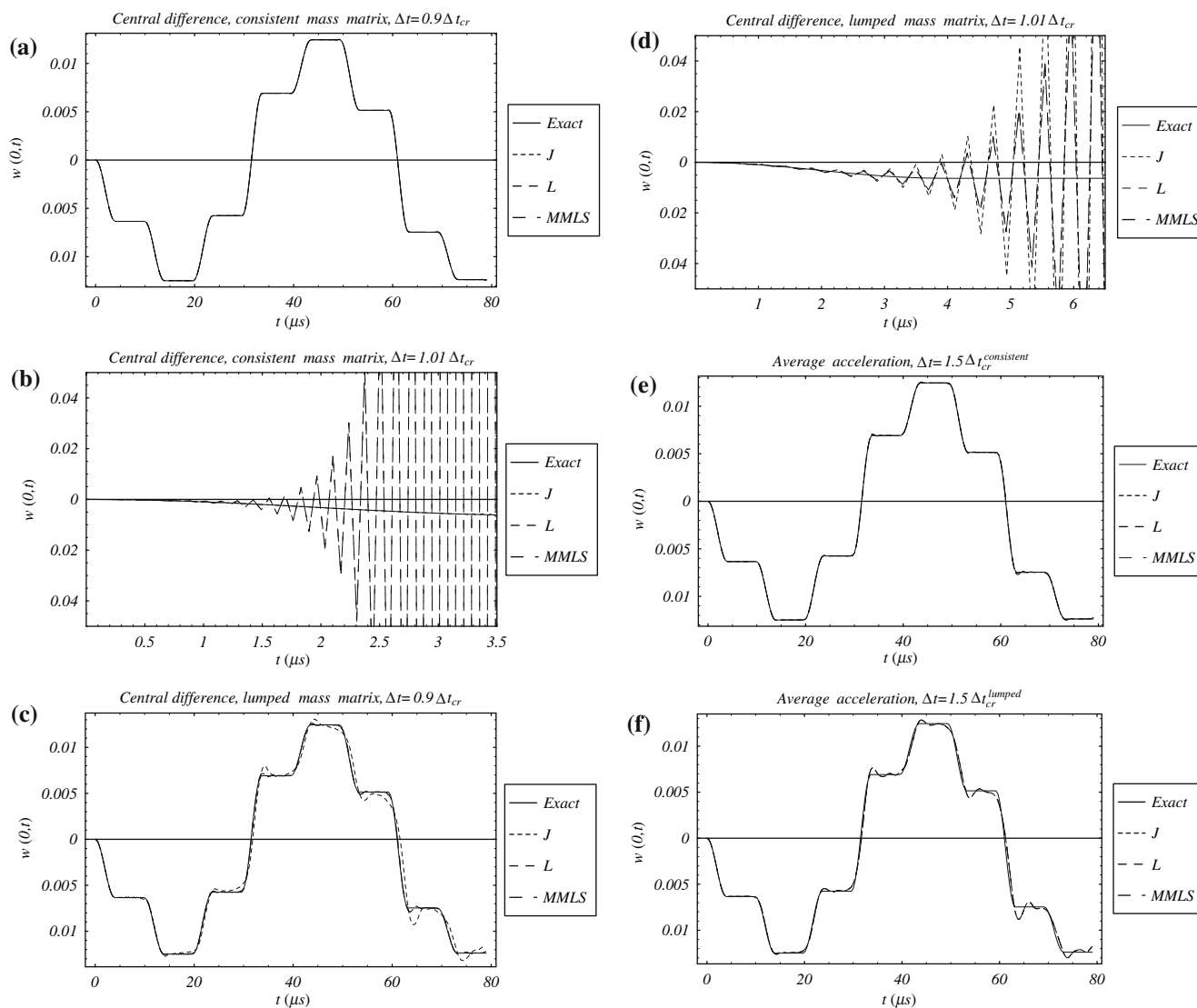


Fig. 13 Time history of the free end displacement obtained with **a** central difference, consistent mass matrix, and $\Delta t = 0.9\Delta t_{cr}$; **b** central difference, consistent mass matrix, and $\Delta t = 1.01\Delta t_{cr}$; **c** central difference, lumped mass matrix, and $\Delta t = 0.9\Delta t_{cr}$; **d** central difference, lumped mass matrix, and $\Delta t = 1.01\Delta t_{cr}$; **e** average acceleration, consistent mass matrix, and $\Delta t = 1.5\Delta t_{cr}^{consistent}$; (**f**) average acceleration, consistent mass matrix, and $\Delta t = 1.5\Delta t_{cr}^{lumped}$

are lower than those in the FE solution. This is a very favorable feature of the MLPG6 method with respect to the FEM; the higher computational time required to evaluate domain integrals is balanced somewhat by a gain in accuracy.

The analysis of the transient response due to an axial traction of finite time duration applied at one end of the bar reveals a very good agreement between the MLPG6, and the analytical solutions. Each technique for the treatment of the material discontinuity is able to capture the wave reflection, and interaction between waves at the interface between two materials. Whereas the method of the special jump function is the most accurate in modeling the continuity of the axial stress at the interface because of the introduction of a dedicated degree of freedom, the size of the support of the jump function significantly affects the accuracy of computed

results. Numerical experiments suggest that, for this problem, about one half of the nodes employed in the discretization of the global domain need to be included in the radius of the support of the jump function in order to ensure good results. For the consistent mass matrix, the critical time step size for the method of jump function is nearly one-half of that for the other two methods. Both the method of Lagrange multipliers, and the MLS discontinuous basis functions can be generalized to more complex geometries involving material discontinuities.

For the lumped mass matrix, the three methods of accounting for the material discontinuity give the same maximum frequency of the segmented bar. However, when the consistent mass matrix is employed, the maximum natural frequency computed with the method of jump function is nearly twice

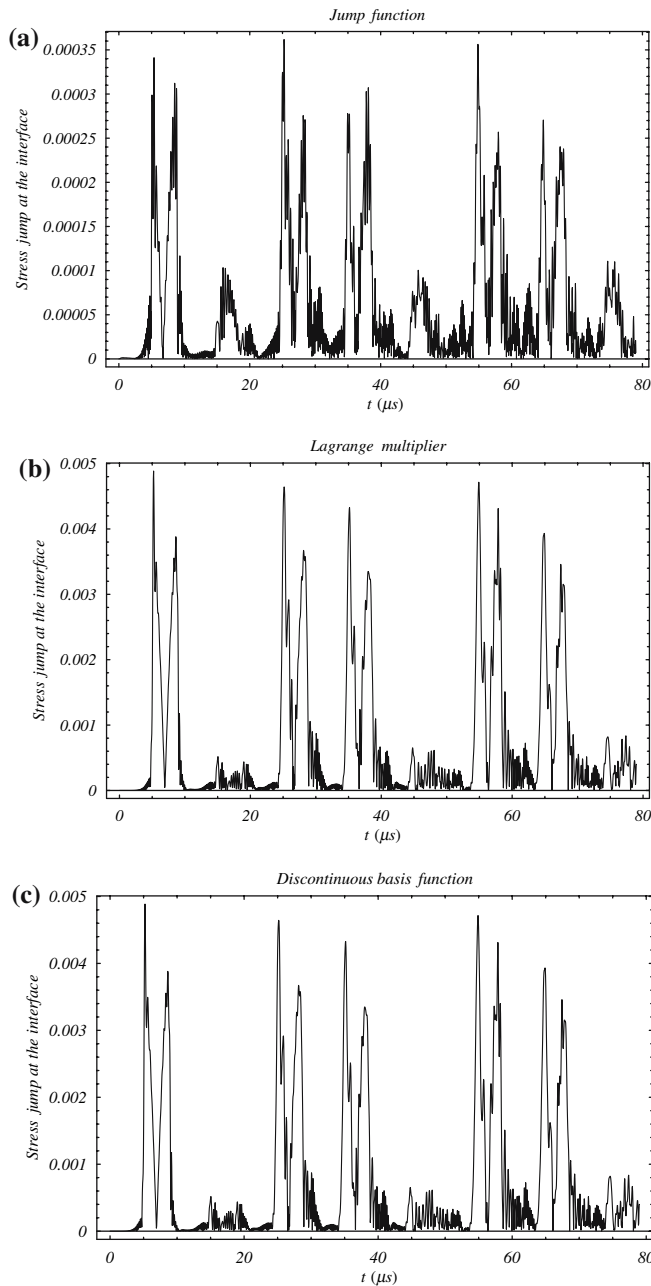


Fig. 14 Time history of the jump in the axial stress at the interface using **a** the special jump function, **b** the Lagrange multiplier, and **c** the modified MLS basis functions with discontinuous derivatives

of that for the other two methods. The largest frequency computed with the lumped mass matrix is nearly one-third of that obtained with the consistent mass matrix. Thus for the explicit time-integration method, it is more efficient to use the lumped mass matrix.

Appendices

We present below analytical solutions for free, and forced vibrations of a segmented bar comprised of two materials.

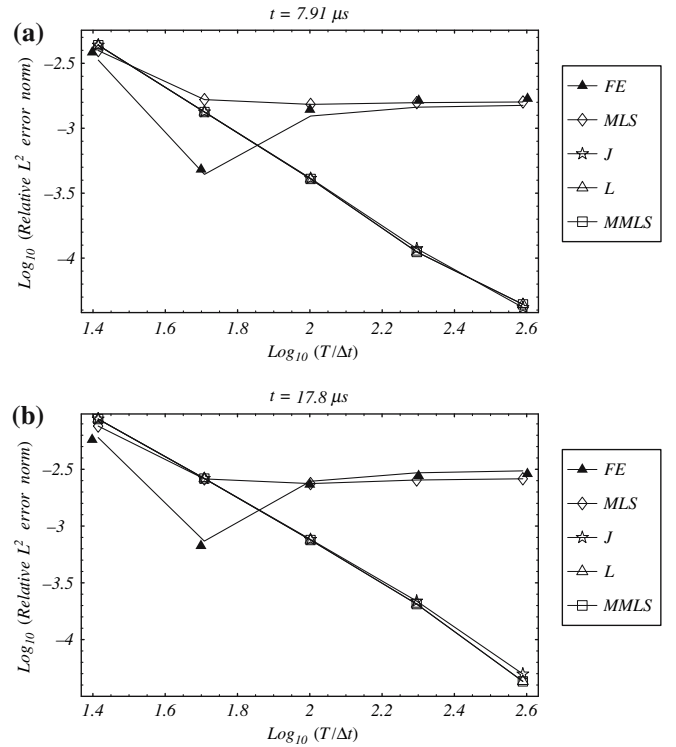


Fig. 15 At two different times, effect of the time step size on the L^2 relative error norm in the axial displacement

A. Free vibrations

We consider in Eqs. (26) and (27) displacement fields of the form

$$w_1(x, t) = W_1(x) \exp(i\omega t), \quad w_2(x, t) = W_2(x) \exp(i\omega t). \quad (94)$$

Imposing homogeneous form of boundary conditions (28), (29), (30), and (31) in (26), (27), we obtain the following transcendental characteristic equation for the frequency ω :

$$\tan\left(\frac{a}{c_1}\omega\right) \tan\left(\frac{L-a}{c_2}\omega\right) = \frac{c_1 E_2}{c_2 E_1}. \quad (95)$$

The corresponding mode shapes are given by

$$W_1(\omega, x) = \gamma(\omega) \cos\left(\frac{\omega}{c_1}x\right), \quad (96)$$

$$W_2(\omega, x) = \gamma(\omega) \frac{\cos\left(\frac{a}{c_1}\omega\right)}{\cos\left(\frac{a}{c_2}\omega\right) \tan\left(\frac{a}{c_2}\omega\right) - \tan\left(\frac{L}{c_2}\omega\right)} \times \left[\sin\left(\frac{\omega x}{c_2}\right) - \tan\left(\frac{\omega L}{c_2}\right) \cos\left(\frac{\omega x}{c_2}\right) \right],$$

where W_1 is defined on $(0, a)$, and W_2 on (a, L) . Adopting the normalization

$$\int_0^a W_1^2(\omega, x) dx + \int_a^L W_2^2(\omega, x) dx = 1, \quad (97)$$

we get

$$\gamma(\omega) = \frac{\omega}{c_1 \sin\left(\frac{L}{c_1}\omega\right) - c_2 \cos\left(\frac{a}{c_2}\omega\right) \tan\left(\frac{L-a}{c_2}\omega\right)}. \quad (98)$$

B. Forced vibrations

Let

$$\begin{aligned} \mathbf{W}_i(x, s) &= \int_0^\infty \exp(-st) w_i(x, t) dt, \\ \mathbf{P}(s) &= \int_0^\infty \exp(-st) p(t) dt, \quad i = 1, 2, \end{aligned} \quad (99)$$

be the one-sided Laplace transforms of w_i and p . Therefore, the system of partial differential equations (26) and (27) in the Laplace domain becomes

$$\frac{\partial^2 \mathbf{W}_i(x, s)}{\partial x^2} - \frac{s^2}{c_i^2} \mathbf{W}_i(x, s) = 0, \quad i = 1, 2, \quad (100)$$

whose general solution is

$$\begin{aligned} \mathbf{W}_i(x, s) &= A_i(s) \exp\left(-\frac{s}{c_i}x\right) + B_i(s) \exp\left(\frac{s}{c_i}x\right), \\ i &= 1, 2, \end{aligned} \quad (101)$$

where two waves propagating in opposite directions are recognized. The four coefficients are determined by imposing the following boundary conditions in the Laplace domain:

$$\begin{aligned} E_1 \frac{\partial \mathbf{W}_1}{\partial x}(0, s) &= \mathbf{P}(s), \\ \mathbf{W}_1(a, s) &= \mathbf{W}_2(a, s), \\ E_1 \frac{\partial \mathbf{W}_1}{\partial x}(a, s) &= E_2 \frac{\partial \mathbf{W}_2}{\partial x}(a, s), \\ \mathbf{W}_2(L, s) &= 0. \end{aligned} \quad (102)$$

Hence we obtain

$$\begin{aligned} A_1(s) &= -\frac{c_1}{E_1} \frac{\alpha \exp\left(-2\frac{L-a}{c_2}s\right) + 1}{1 + \Xi(s)} \frac{\mathbf{P}(s)}{s}, \\ B_1(s) &= \frac{c_1}{E_1} \frac{\alpha \exp\left(-2\frac{a}{c_1}s\right) + \exp\left(-2\left(\frac{a}{c_1} + \frac{L-a}{c_2}\right)s\right)}{1 + \Xi(s)} \\ &\quad \times \frac{\mathbf{P}(s)}{s}, \\ A_2(s) &= -2 \frac{c_1 c_2}{c_1 E_2 + c_2 E_1} \frac{\exp\left(\left(\frac{a}{c_2} - \frac{a}{c_1}\right)s\right)}{1 + \Xi(s)} \frac{\mathbf{P}(s)}{s}, \\ B_2(s) &= 2 \frac{c_1 c_2}{c_1 E_2 + c_2 E_1} \frac{\exp\left(-\left(\frac{a}{c_1} + \frac{2L-a}{c_2}\right)s\right)}{1 + \Xi(s)} \frac{\mathbf{P}(s)}{s}, \end{aligned} \quad (103)$$

where the constant $\alpha = \frac{c_1 E_2 - c_2 E_1}{c_1 E_2 + c_2 E_1}$ and the function

$$\begin{aligned} \Xi(s) &= \exp\left(-2\left(\frac{a}{c_1} + \frac{L-a}{c_2}\right)s\right) \\ &\quad + \alpha \exp\left(-2\frac{L-a}{c_2}s\right) + \alpha \exp\left(-2\frac{a}{c_1}s\right), \end{aligned} \quad (104)$$

have been introduced. Identifying the term $\frac{1}{1 + \Xi(s)}$ as the sum of the corresponding geometric series, we write

$$\frac{1}{1 + \Xi(s)} = \sum_{j=0}^{\infty} [-\Xi(s)]^j \quad (105)$$

$$\begin{aligned} &= \sum_{j=0}^{\infty} \sum_{k=0}^j \sum_{h=0}^k \binom{j}{k} \binom{k}{h} (-1)^j \alpha^k \\ &\quad \times \exp\left(-2\left(\frac{(j-k+h)a}{c_1} + \frac{(j-h)(L-a)}{c_2}\right)s\right). \end{aligned}$$

Therefore, solutions are given by

$$\mathbf{W}_i(x, s) = G_i(x, s) \mathbf{P}(s), \quad (106)$$

where

$$\begin{aligned} G_1(x, s) &= \frac{c_1}{s E_1} \sum_{j=0}^{\infty} \sum_{k=0}^j \sum_{h=0}^k \binom{j}{k} \binom{k}{h} \\ &\quad \times \left\{ (-1)^{j+1} \left[\alpha^{k+1} \exp\left(-2\left(\frac{(j-k+h)a}{c_1} + \frac{(j-h+1)(L-a)}{c_2} + \frac{x}{2c_1}\right)s\right) \right. \right. \\ &\quad \left. \left. + \alpha^k \exp\left(-2\left(\frac{(j-k+h)a}{c_1} + \frac{(j-h)(L-a)}{c_2} + \frac{x}{2c_1}\right)s\right) \right] \right. \\ &\quad \left. + (-1)^j \left[\alpha^{k+1} \exp\left(-2\left(\frac{(j-k+h+1)a}{c_1} + \frac{(j-h)(L-a)}{c_2} - \frac{x}{2c_1}\right)s\right) \right. \right. \\ &\quad \left. \left. + \alpha^k \exp\left(-2\left(\frac{(j-k+h+1)a}{c_1} + \frac{(j-h+1)(L-a)}{c_2} - \frac{x}{2c_1}\right)s\right) \right] \right\}, \end{aligned} \quad (107)$$

and

$$G_2(x, s) = \frac{2c_1c_2}{s(c_1E_2 + c_2E_1)} \sum_{j=0}^{\infty} \sum_{k=0}^j \sum_{h=0}^k \binom{j}{k} \binom{k}{h} \alpha^k \times \left\{ (-1)^{j+1} \exp\left(-2\left(\frac{(j-k+h)a}{c_1} + \frac{(j-h)(L-a)}{c_2} + \frac{x-a}{2c_2} + \frac{a}{2c_1}\right)s\right) + (-1)^j \exp\left(-2\left(\frac{(j-k+h)a}{c_1} + \frac{(j-h)(L-a)}{c_2} + \frac{a}{2c_1} + \frac{2L-a-x}{2c_2}\right)s\right) \right\}, \tag{108}$$

are the transfer functions. From the shifting theorem in the real domain (see e.g., [22]) the inverse Laplace transforms $g_1(x, t)$ and $g_2(x, t)$ of the transfer functions are easily found. Using the convolution theorem [22], the axial deflections in the time domain are given by

$$w_i(x, t) = \int_0^t g_i(x, t - \vartheta) p(\vartheta) d\vartheta, \quad i = 1, 2.$$

Recalling the expression (34) for $p(t)$ we obtain

$$w_1(x, t) = \frac{c_1PT}{\pi E_1} \sum_{j=0}^{\infty} \sum_{k=0}^j \sum_{h=0}^k \binom{j}{k} \binom{k}{h} \alpha^k \times \left\{ (-1)^{j+1} \left[\alpha^{k+1} \zeta\left(t - 2\left(\frac{(j-k+h)a}{c_1} + \frac{(j-h+1)(L-a)}{c_2} + \frac{x}{2c_1}\right)\right) + \alpha^k \zeta\left(t - 2\left(\frac{(j-k+h)a}{c_1} + \frac{(j-h)(L-a)}{c_2} + \frac{x}{2c_1}\right)\right) \right] + (-1)^j \left[\alpha^{k+1} \zeta\left(t - 2\left(\frac{(j-k+h+1)a}{c_1} + \frac{(j-h)(L-a)}{c_2} - \frac{x}{2c_1}\right)\right) + \alpha^k \zeta\left(t - 2\left(\frac{(j-k+h+1)a}{c_1} + \frac{(j-h+1)(L-a)}{c_2} - \frac{x}{2c_1}\right)\right) \right] \right\}, \tag{109}$$

$$w_2(x, t) = \frac{2c_1c_2PT}{\pi(c_1E_2 + c_2E_1)} \sum_{j=0}^{\infty} \sum_{k=0}^j \sum_{h=0}^k \binom{j}{k} \binom{k}{h} \alpha^k \times \left\{ (-1)^{j+1} \zeta\left(t - 2\left(\frac{(j-k+h)a}{c_1} + \frac{(j-h)(L-a)}{c_2} + \frac{x-a}{2c_2} + \frac{a}{2c_1}\right)\right) + (-1)^j \zeta\left(t - 2\left(\frac{(j-k+h)a}{c_1} + \frac{(j-h)(L-a)}{c_2} + \frac{a}{2c_1} + \frac{2L-a-x}{2c_2}\right)\right) \right\}, \tag{110}$$

$$+ (-1)^j \zeta\left(t - 2\left(\frac{(j-k+h)a}{c_1} + \frac{(j-h)(L-a)}{c_2} + \frac{a}{2c_1} + \frac{2L-a-x}{2c_2}\right)\right),$$

where

$$\zeta(\beta) := \begin{cases} \left(1 - \cos\frac{\pi\beta}{T}\right) \mathcal{H}(\beta), & \beta < T \\ 2\mathcal{H}(\beta), & \beta \geq T \end{cases}, \quad \beta \in \mathbb{R}. \tag{111}$$

Obviously, $w_1(x, t)$ holds for $x \in (0, a)$, and $w_2(x, t)$ for $x \in (a, L)$.

Acknowledgements This work was partially supported by the ONR grant N00014-98-01-0300 with Dr. Y. D. S. Rajapakse as the program manager. Views expressed herein are those of authors, and neither of the funding agency nor of Virginia Polytechnic Institute and State University.

References

1. Andreus U, Batra RC, Porfiri M (2005) Vibrations of cracked Euler-Bernoulli beams using meshless local Petrov-Galerkin (MLPG) method. CMES: Comput Model Eng Sci 9:111-132
2. Atluri SN, Shen SP (2002) The meshless local Petrov-Galerkin method. Tech. Science Press, California
3. Atluri SN, Zhu T (1998) A new meshless local Petrov-Galerkin (MLPG) approach in computational mechanics. Comput Mech 22:2117-2127
4. Atluri SN, Cho JY, Kim H-G (1999) Analysis of thin beams, using the meshless local Petrov-Galerkin method, with generalized moving least squares interpolations. Comput Mech 24:334-347
5. Bathe KJ (1996) Finite element procedures. Prentice-Hall, Englewood Cliffs
6. Batra RC, Vidoli S (2002) Higher order piezoelectric plate theory derived from a three-dimensional variational principle. AIAA J 40(1):91-104
7. Batra RC, Wright TW (1986) Steady state penetration of rigid perfectly plastic targets. Int J Eng Sci 24(1):41-54
8. Batra R, Porfiri M, Spinello D (2004) Treatment of material discontinuity in two meshless local Petrov-Galerkin (MLPG) formulations of axisymmetric transient heat conduction. Int J Numer Methods Eng 61:2461-2479
9. Belytschko T, Fish J, Engelman BE (1988) A finite-element with embedded localization zones. Comput Methods Appl Mech Eng 70:59-89
10. Belytschko T, Lu YY, Gu L (1994) Element-free Galerkin methods. Int J Numer Methods Eng 37:229-256
11. Cordes LW, Moran B (1996) Treatment of material discontinuity in the element-free Galerkin method. Comput Methods Appl Mech Eng 139:75-89
12. Duarte CAM, Oden JT (1996) Hp clouds - an hp meshless method. Numer Methods Partial Differential Equations 12:673-705
13. Gu YT, Liu GR (2001) A meshless local Petrov-Galerkin (MLPG) method for free and forced vibration analyses for solids. Comput Mech 27:188-198
14. Hughes TJR (2001) The finite element method. Linear static and dynamic finite element analysis. Prentice-Hall, New Jersey
15. Kansa EJ (1990) Multiquadrics - A scattered data approximation scheme with applications to computational fluid dynamics. ii: Solutions to parabolic, hyperbolic and elliptic partial differential equations. Comput Math Appl 19:147-161
16. Kim H-G, Atluri SN (2000) Arbitrary placement of secondary nodes, and error control, in the meshless local Petrov-Galerkin (MLPG) method. CMES: Comput Model Eng Sci 1:11-32

17. Krongauz Y, Belytschko T (1998) EFG approximation with discontinuous derivatives. *Int J Numer Methods Eng* 41:1215–1233
18. Lancaster P, Salkauskas K (1981) Surfaces generated by moving least squares methods. *Math Comput* 37:141–158
19. Liu GR (2003) *Mesh free methods*. CRC Press, Boca Raton
20. Liu WK, Jun S, Adee J, Belytschko, T (1995) Reproducing kernel particle methods for structural dynamics. *Int J Numer Methods Eng* 38:1655–1679
21. Lucy LB (1977) A numerical approach to the testing of the fission hypothesis. *Astron J* 82:1013–1024
22. Meirovitch L (2001) *Fundamentals of vibrations*. McGraw Hill, New York
23. Melenk JM, Babuska I (1996) The partition of unity finite element method: basic theory and applications. *Comput Methods Appl Mech Eng* 139:289–314
24. Mura T, Koya T (1992) *Variational methods in mechanics*. Oxford University Press, New York
25. Nayroles B, Touzot G, Villon P (1992) Generalizing the finite element method: diffuse approximation and diffuse elements. *Comput Mech* 10:307–318
26. Noguchi H, Sachiko M (2006) Analysis of structure with material interface by meshfree method. *CMES: Comput Model Eng Sci* (in press)
27. Qian LF, Batra RC, Chen LM (2003a) Elastostatic deformations of a thick plate by using higher-order shear and normal deformable plate theory and two meshless local Petrov–Galerkin (MLPG) methods. *CMES: Comput Model Eng Sci* 4:161–176
28. Qian LF, Batra RC, Chen LM (2003b) Free and forced vibrations of thick rectangular plates by using higher-order shear and normal deformable plate theory and meshless local Petrov–Galerkin (MLPG) method. *CMES: Comput Model Eng Sci* 4:519–534
29. Qian LF, Batra RC (2004a) Transient thermoelastic deformations of a thick functionally graded plate. *J Therm Stress* 27:705–740
30. Qian LF, Batra RC, Chen LM (2004b) Static and dynamic deformations of a thick functionally graded elastic plate by using a higher-order shear and normal deformable plate theory and meshless local Petrov–Galerkin (MLPG) method. *Composites B* 35:685–697
31. Sukumar N, Moran B, Belytschko T (1998) The natural element method in solid mechanics. *Int J Numer Methods Eng* 43:839–887
32. Vidoli S, Batra RC (2000) Derivation of plate and rod equations for a piezoelectric body from a three-dimensional variational principle. *J Elast* 59:23–50
33. Warlock A, Ching H-K, Kapila AK, Batra RC (2002) Plane strain deformations of an elastic material compressed in a rough rectangular cavity. *Int J Eng Sci* 40:991–1010
34. Wendland H (1995) Piecewise polynomial, positive definite and compactly supported radial basis functions of minimal degree. *Adv Comput Math* 4:389–396
35. Zhang GM, Batra RC (2004) Modified smoothed particle hydrodynamics method and its application to transient problems. *Comput Mech* 34:137–146
36. Zhang GM, Batra RC (2006) Symmetric smoothed particle hydrodynamics (SSPH) method, and selection of the Kernel function. (in press)